UNIVERSITETET I BERGEN

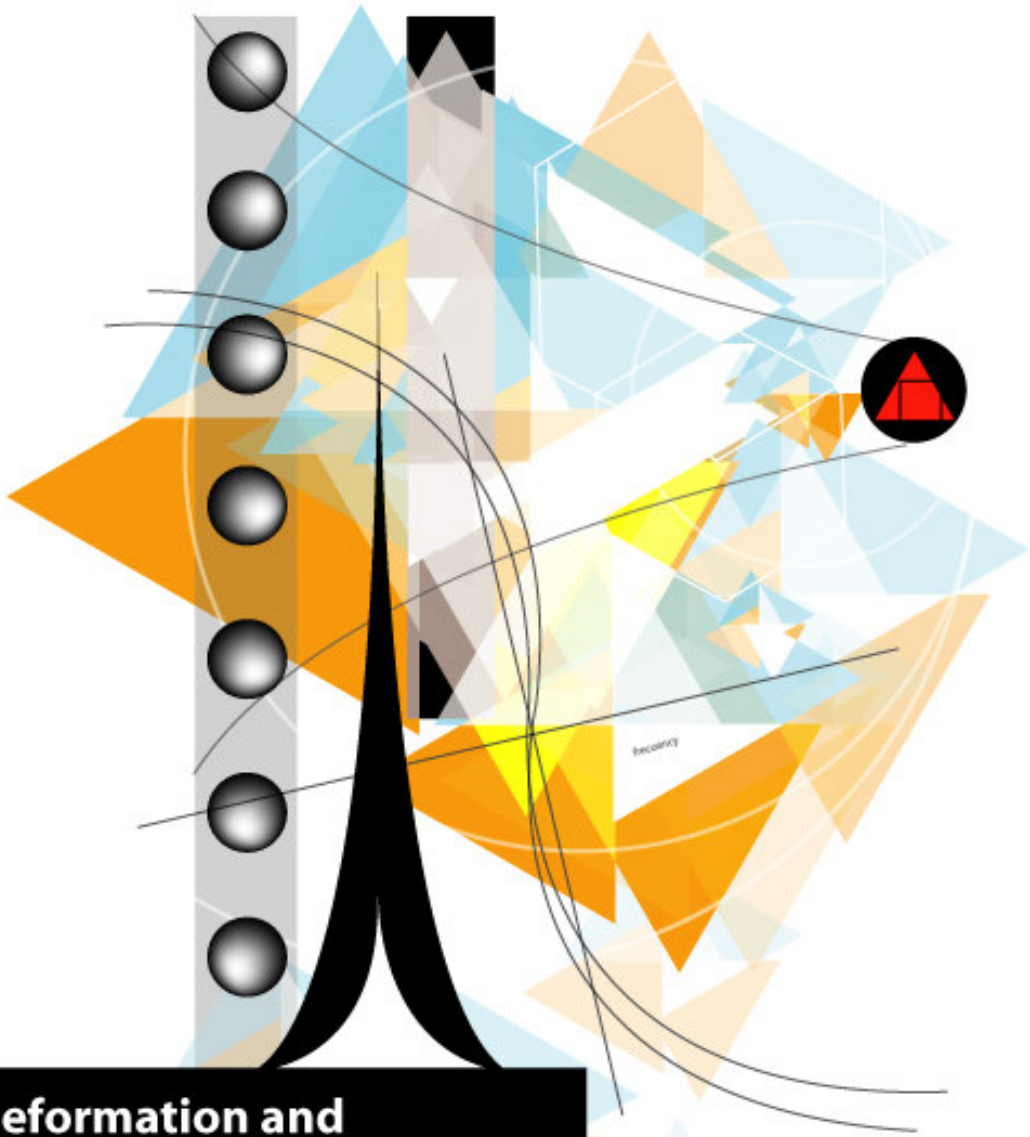

Crustal deformation and attenuation in Venezuela

Carolina Granado Ruiz.

University of Bergen. Department of Earth Science. Geodynamics Group.

A dissertation for the Master Degree in Seismology
June 2005

Crustal deformation and attenuation in Venezuela

A DISSERTATION SUBMITTED TO THE DEPARTMENT OF EARTH SCIENCE OF THE UNIVERSITY OF BERGEN IN PARTIAL FULFILMENT OF THE REQUIREMENTS FOR A MASTER'S DEGREE IN SEISMOLOGY

Carolina Granado Ruiz
Bergen
June 2005

Crustal deformation and attenuation in Venezuela

By

Carolina Granado Ruiz

This thesis is based on two papers. The two papers are listed below and are unpublished manuscripts:

Paper I: Granado, C., Atakan, K. Transcurrent deformation along Venezuela based on the stress inversion of focal mechanisms.

Paper II: Granado, C., Havskov, J. Near surface attenuation in Venezuela.

Contents

Introduction

The purpose of this thesis is to make use of new seismic data in Venezuela in order to improve seismology practice. The theses will focus on two topics: stress inversion and seismic attenuation.

1. The first paper, contained in this thesis, aims to provide new analysis regarding the tectonic deformation of Venezuela as a complex result of the interaction of three major plates, the Caribbean, South America and Nazca plates. The paper is based on inversion of focal mechanism based on the method developed by Michael (References in paper I, 1987, 1984). In addition, currently available geologically derived data is used. .
2. The second paper focuses on an area of quality control in seismological data interpretation that is not currently undertaken in Venezuela. Imprecise estimates of the near surface attenuation affect the accuracy of earthquake source parameters. Accurate attenuation estimate is a key parameter when determining corner frequency by spectral analysis of small earthquakes. This paper determines currently unavailable data on near-surface attenuation in Venezuela, to serve as input to calculations on local seismological measurements.

Transcurrent deformation along Venezuela based on the stress inversion of focal mechanisms

This paper analyses tectonic deformation of Venezuela as a complex result of the interaction of three major plates; the Caribbean, South America and Nazca plates. The analysis is based on inversion of focal mechanism based on a method developed by Michael (References in paper I, 1987, 1984). Stress inversions of earthquake focal mechanisms help determine crustal tectonic stress distributions and study their implications in kinematics processes.

We divide the area into eight zones, based on the location of active faults in the Venezuela region, and study regional stress field variations along the entire region from East to West.

A dataset of 125 events is distributed along segments of mainly three fault systems; (1) Eastern, (2) Central and (3) Western. Sample variance ranges from 0.15 to 0.28. Certain offshore data points in the Central region are ignored, as they seem to belong to a different tectonic structure not involved in the kinematics processes studied here.

Inversion of the data set (all 125 events) indicates a clear strike slip faulting regime with σ_1 oriented almost horizontally in the NW-SE direction, while significant variations are seen locally among the three major fault systems. In all three fault systems the dominant faulting regime is strike slip ($S_H > S_V > S_h$). However, both the orientation of σ_1 and its plunge varies from the eastern parts of Venezuela (plunging SE with a NW-SE

azimuth), to the central parts (plunging N, with N-S azimuth), and finally to the west (plunging NW with a WW-SE azimuth).

These results correlate with the general plate motions and associated deformations in the Venezuelan area. The observed dynamics accommodate the lateral transition from westerly dipping subduction in the North west to easterly dipping subduction in the south west through predominantly strike slip faulting along the three main systems; the El Pilar fault system in the east, the San Sebastián and La Victoria fault systems in the central area and Boconó fault system in the west.

Near surface attenuation in Venezuela

Accuracy in determining source parameters of earthquakes depends on estimates regarding the decrease in amplitude of seismic waves as they propagate through the earth surface. We perform spectral analysis on earthquake events in Venezuela to analyze near surface attenuation. The data put forth in this study can thus provide an element of quality control in seismological analysis not currently undertaken in Venezuela.

The study is based on 200 earthquakes in Venezuela, with epicentral distances of less than 100 km and magnitudes from 1.1 to 2.5 Mw. The earthquakes were recorded at 100 samples per second by means of vertical component seismograms in broad band stations, between 1 July and 15 December 2003. Only vertical component seismograms were employed. The Venezuelan Foundation for Seismological Research (FUNVISIS) made the data available. Values for near surface attenuation in the Caribbean are used for comparison.

In earthquake scaling calculations, quality factor Q plays a central role. Q generally has a very low value immediately below the surface, rapidly increasing with depth. Since almost no Q-values are known for Venezuela, a preliminary coda Q study is done, using the standard coda-q method. We observe that Q increases with frequency as well as with time window length, which is taken into account in further calculations.

Attenuation closed to seismic stations is described by the near-surface attenuation parameter (κ). κ is critical in determining a reliable source corner frequency for small earthquakes. Near surface attenuation is strongest for high frequencies. Thus, near surface attenuation affect the displacement spectrum showing lower corner frequency than the frequency that actually characterise the earthquake.

We use an empirical relation to control the data for corner frequency. The most reliable Q results were taken to calculate κ in a frequency band from 3 -12 Hz.

No significant variations in average κ for different coda Q relations have been observed. Some regional variations in κ are seen, pointing to possible differences in local geological conditions at the measuring stations.

The study concludes on an average value of near surface attenuation κ of 0.099 ± 0.031 with $Q=65f^{0.84}$, implying that surface attenuation in Venezuela is significantly stronger than in other regions in America. These findings imply a dramatic effect on the estimation of the corner frequency in spectral analysis of smaller earthquakes in Venezuela.

Acknowledgements

I would like to thank my supervisors Jens Havskov and Kuvvet Atakan for offering me an interesting subject and for their help throughout the process of writing scientific articles.

I would like to thank my student fellows at the Department of Earth Sciences for their company. I forward my gratitude especially to Zoya Zarifi and Mohammed Raeesi for interesting discussions in several topics, from science to life. Tsoja Wangmo and Ciring Cering for being sweet and kind people.

I thank my colleagues in FUNVISIS and the institution itself for their assistance. In particular, Franck Audemard for allowing me to access his valuable paper collection, Gloria Romero for her collaborative enthusiasm and support regarding the use of FUNVISIS data base, José Antonio Rodríguez for being my favourite gentleman always helpful. Carola Guillén, Betty Escalona and Xiomelys Campo for their kindness. Raquel Vásquez and Leonardo Alvarado for their help and for being good fellows. Rafael Dávila for his technical support. Special mention to Daniel Moreno who was always there for helping me and for being a competent professional and best friend.

I want to express my gratitude to Monika Sobiesiak who is a source of inspiration to me and who gave me valuable lessons.

During my studies in Bergen, I met a lot of people that I need to thank for their valuable help and outstanding friendship. Iviana thanks for being my sunshine, Tone thanks for being my beautiful Norwegian friend, Sajo thanks for being my sister, Saleh you are my brother,

Christine thanks for being sweet and cooking so well. Thanks To Jannicke, Carole and Rianne for their friendship.

My master studies have been financed by the Venezuelan National Fond for Science and Technology (FONACIT) and travel assistance has been received from FUNVISIS (Venezuelan Foundation for Seismological Research).

Thanks to my friends in Venezuela for helping me, Girola, Cloritza, Ana Jagui, Maru and Ivette, girls you are wonderful. There is always an "añomaño" to keep in my mind.

Finally, I thank my family for encouraging me and always being there and caring for me in every possible way in these difficult years. I dedicated this effort in particular to Juan José and Dorotea for giving me strength and my loving Felicia, Joan and Idana.

Transcurrent deformation along Venezuela based on the stress inversion of focal mechanisms

Carolina Granado and Kuvvet Atakan

Abstract

This paper analyses tectonic deformation of Venezuela as a complex result of the interaction of three major plates; the Caribbean, South America and Nazca plates. The analysis is based on inversion of focal mechanism based on a method developed by Michael (1987, 1984). Stress inversions of earthquake focal mechanisms help determine crustal tectonic stress distributions and study their implications in kinematics processes. Inversion of the data set (all 125 events) indicates a clear strike slip faulting regime with σ_1 oriented almost horizontally in the NW-SE direction, while significant variations are seen locally among the three major fault systems. These results correlate with the general plate motions and associated deformations in the Venezuela area. The observed dynamics accommodate the lateral transition from westerly dipping subduction in the north west to easterly dipping subduction in the south west through predominantly strike slip faulting along the three main systems; the El Pilar fault system in the East, the San Sebastián and La Victoria fault systems in the Central area and Boconó fault system in the west.

1.- Introduction

The geodynamic setting of the southern Caribbean and north western part of South America shows a deformation as a result of the interaction of four major plates: South America, Nazca, Cocos and Caribbean plates. Kinematic studies based on GPS between the Caribbean and South America show that considering fixed the South American

plate, the Caribbean plate motion is towards the east-southeast, while the Nazca plate motion is towards the east and the northern Andes motion is towards the northeast (Corredor, 2003). The main component of the Caribbean plate is a large volcanic plateau probably formed in the Pacific Ocean and there is evidence of a relative displacement between Colombia and Venezuela microplates (Leroy and Mauffret, 1996).

This setting defines the entire deformation of Venezuela as a part of a transcurrent boundary with transition to convergent boundaries both in east and west boundaries where subduction processes are taking place with opposite polarity, i.e westerly dipping subduction of the Atlantic under the Caribbean plate and easterly dipping subduction of the Nazca plate under the South America plate (Figure 1)

A similar situation where a tectonic transition with polarity changes through a transcurrent zone occurs in New Zealand. In this region, a west dipping subduction off shore in the North island changes to an east dipping subduction in the South island forming the Alpine Fault System (Sutherland, 1999).

Our motivation is to understand the process occurring along the transition from the pure subduction to pure strike slip transcurrent deformation. This can be studied in mainly three geological areas around the Caribbean. In the NE, the transition from the subduction in the Greater Antilles to the transcurrent deformation south of Cuba (Moreno et al, 2002) occurs in a broader zone of deformation including the Northern part of Haiti and Dominican Republic and partly also Jamaica (Grandison and Atakan, 2005).

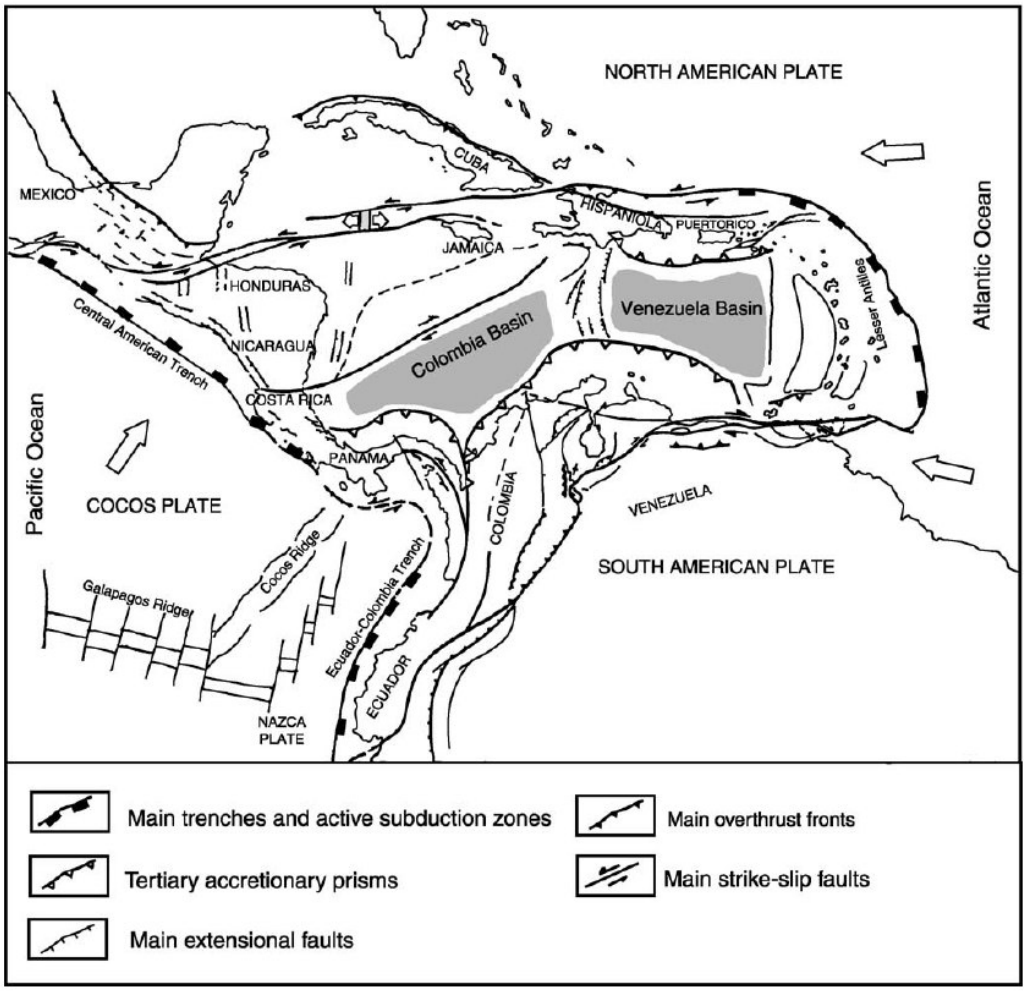

Figure 1: Structural sketch map of the Caribbean area (Giunta et al, 2002).

In the SW part of the Caribbean, the transition from the subduction along the Northern Andes to the transcurrent deformation in Venezuela occurs in a complex manner involving also the influence of the Cocos and Nazca plates. This gives rise to the development of two deforming belts along the Northern Panamá Deformed Belt and the South Caribbean deformation Zone. In this area the transcurrent motion is probably accommodated by the Boconó fault as well as the Oca-Ancón and Bucaramanga faults (Corredor, 2003; Cortés and Angelier, 2005)

The southern part of the Caribbean plate is the third area where such a transition from subduction to transcurrent deformation occurs.

In the easternmost Venezuela, the subduction along the Lesser Antilles gradually changes into on strike slip system, of faults starting from Trinidad across El Pilar fault and joins into the San Sebastián and la Victoria fault systems in Central Venezuela.

Quaternary fault kinematics and stress tensor along this area has recently been reviewed by Audemard et al (2005). These results are based on detailed analysis of individual fault slip data including also the focal mechanisms of recent earthquakes. However, no attempt has been made to obtain the stress tensor by inversion of the existing fault plane solutions.

In this study, we address the problem by inverting the focal mechanisms for finding out the regional system tensor and its variation along the entire Venezuela area.

In this article a data set of 125 focal mechanisms based on P-wave first motion compiled by FUNVISIS (Venezuelan Foundation for Seismological Research) (Romero et al, 2002) in major quaternary faults of Venezuela, is analyzed to determine stress state by inversion of focal mechanisms according to the method proposed by Michael (1984). The results are then compared with solutions obtained by fault slip data compiled for Venezuela (Audemard et al 2005) and the results from the World Stress Map Project (Fig 3) for the Venezuelan region under consideration.

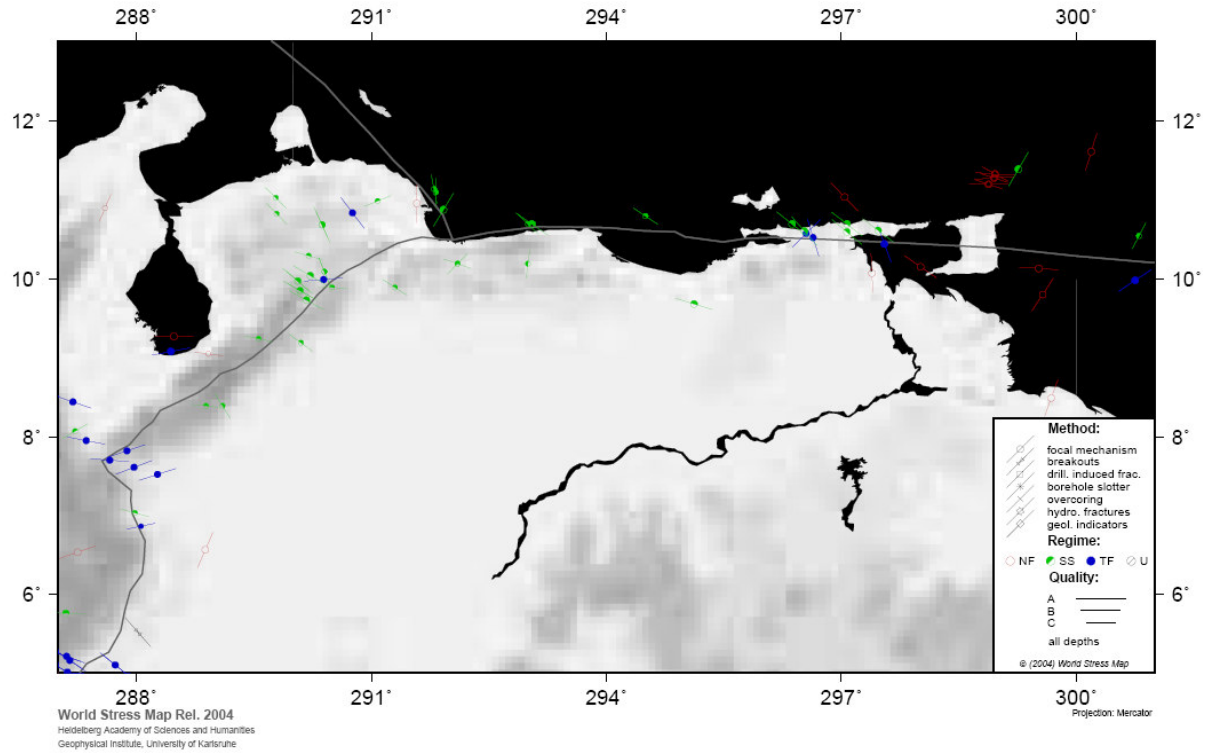

Figure 2: Regional Stress field for Venezuela from World Stress Map Project.
(http://www.world-stress-map.org)

2.- Major Venezuelan active faults and Seismicity

The seismicity and tectonic of Venezuela is basically produced by the interaction zone between the South America and Caribbean plates and the western part of Venezuela shows a complex geodynamic due to plate and block motions producing a broad zone of continental deformation in the Venezuelan Andes characterized by a pattern of thrust and strike-slip fault earthquakes.

The majority of seismic events are crustal, with depths less than 45 km. However, in the north eastern Venezuela, the subduction between the Caribbean and South American plates produce deeper events that can reach up to 120 km (Sobiesiak et al, 2002). The western seismicity is shallow but national and regional networks in Venezuela and Colombia can detect deep earthquakes forming a cluster in the Bucaramanga area.

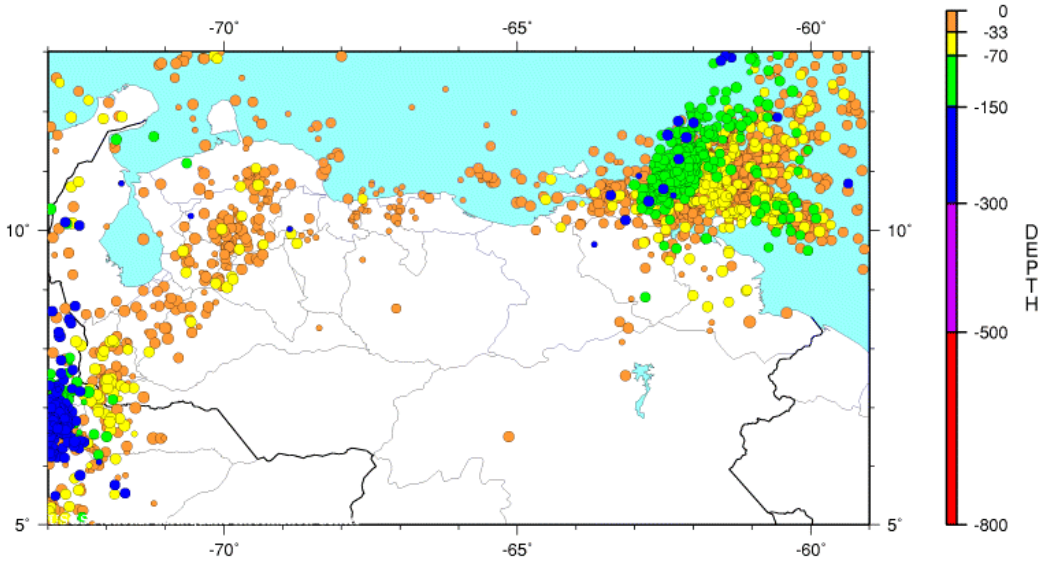

Figure 3: Venezuelan instrumental seismicity between 1973 and April 2005. USGS Catalogue.

The most active faults in Venezuela can roughly be gathered in four main fault systems: A SW-NE trending Mérida Andes known as Boconó fault, EW trending Oca-Ancón fault system in the west, San Sebastian and La Victoria faults in Central Venezuela and El Pilar fault in the east.

Boconó Fault system

The NE-SW trending Boconó fault is slightly oblique to the main Venezuelan Andes axis and bounds the Caribbean Coast range of northern Venezuela on the west. It has an extension tending for about 500 km between the Táchira depression, at the border between Colombia and Venezuela, and Moron, placed in the Caribbean coast of Venezuela.

The Boconó fault presents a 45° bend that allows prolongation into the east-west striking San Sebastian and El Pilar systems. At least five different seismogenic segments have been identified along the Boconó fault based on past seismic activity and potential geometric barriers (Audemard 1999).

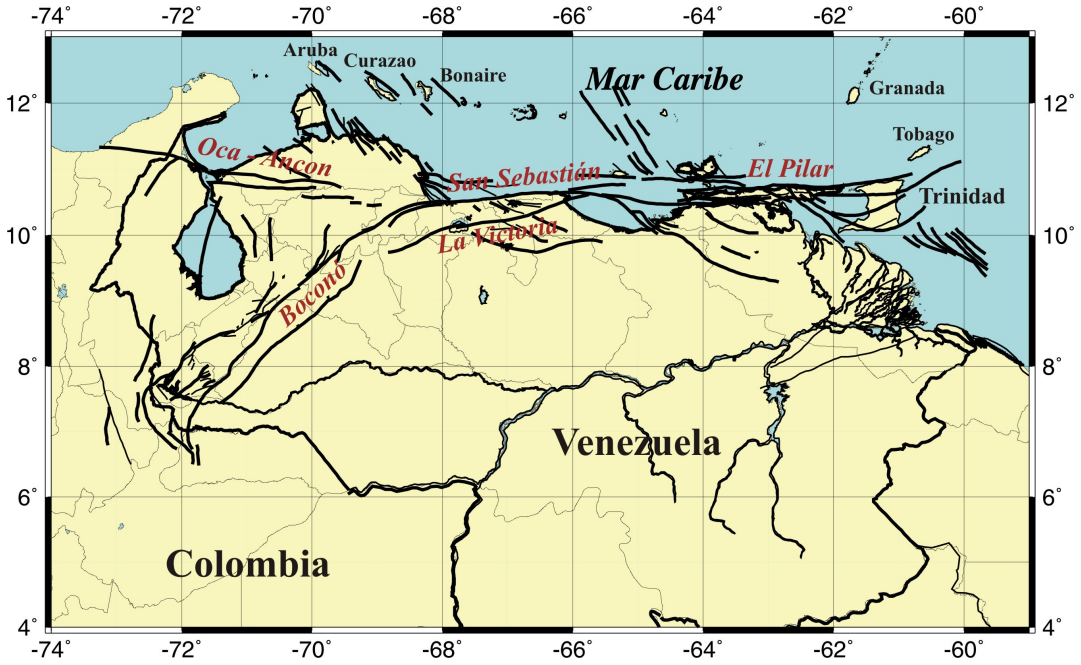

Figure 4: Venezuela main fault systems compiled by FUNVISIS based on Beltrán, 1993

The Boconó fault exhibits a continuous series of aligned 1-5 km wide valleys and linear depressions, passes, saddles, trenches, scarps and sharp ridges (Casas 1991, Ferrer 1991, Singer and Beltran 1996, Audemard 2000). Around 30 km of dextral offsets in Mesozoic rocks have been measured (Giraldo 1989, Audemard and Giraldo 1997). Offset of Quaternary features such as mountainous ridges, drainages, alluvial deposits and shutter ridges varying between 60 and 1000 m depending upon their age.

The Quaternary slip rate is estimated for recent studies in the area between 5 to 9 mm/yr based on 60 to 100 m of dextral offset at Los Zerpas moraines which according to radiocarbon dated a minimum of 13000 years old. These rates are essentially consistent with those predicted by late motions models of about 1 cm/year, assuming that the Boconó fault is part of the main boundary between the Caribbean and South American plates (Freymueler et al 1993).

The Boconó fault slip decreases towards both ends. South of where the fault is the fastest, average slip rate decreases to 5.2 ± 0.9 mm/yr between Mérida and San Cristobal (Audemard 2000) and it is around 1 mm/yr close to the Venezuela Colombia border (Singer and Beltran 1996). The Boconó fault is seismically very active where most of the largest earthquakes in Venezuela took place.

The actual seismicity along the Boconó Fault occurs within a broad zone that generally comprises the entire width of the Mérida Andes, suggesting also that other faults may be also seismogenic, such as the thrust structures building up the mountain chain. For instance, The Guanare March 05, 1975 mb =5.5 and the Ospino December 11, 1977 mb=5.6 are earthquakes associated to the southern Andean Foothills thrust system known as Piedemonte Oriental Fault (Audemard, 2000).

The Oca-Ancón system

The east-west, right-lateral Oca-Ancón fault system extends for 650 km from Santa Marta (Colombia) to Boca de Aroa (eastern coast of Falcon State in Venezuela). This fault used to be part of the plate boundary before being relayed at about 5-3 Ma by the Boconó fault (Audemard 2000). It can be divided in five different sections (Audemard 2000):

Between Santa Marta in Colombia and the outlet of Maracaibo lake (Venezuela): this segment is the simplest and comprises a single trace that truncates the northern part of Perijá range. Westward, it seems to control the linear northern coast of the Sierra Nevada de Santa Marta, and farther west it seems to connect to the east-west striking Jordan fault, estas of Santa Marta. Between Maracaibo lake and Mene de Mauroa: this segment is composed fo two subparallel formations: the east-west striking Oca and Ancón faults. Both traces defined a Quaternary alluvial terrace that limit a large area of probable subsidence that is interpreted as an active pull-apart basin (Audemard, 2000)

Between Mene de Mauroa and Paraíso: this segment is geometrically complex as several strands converge on or diverge from the main lineament. The eastern part of the segment, between Camare and Paraiso in central Falcon, coincides with the Camaro-Paraiso range.

The inner deformation in the fault zone is of strike slip type whereas the outer deformation is characterized by reverse faults leading to consider the whole area as a flower structure.

Between Paraíso and the Aroa valley: this segment strikes WNW-ESE and it comprises several subparallel fault strands of relatively short length in comparison with other segments.

The observed seismic activity consists of small to moderate earthquakes.

Between Socremo and Boca de Aroa: this segment of the fault system regains its original strike along the northern margin of the Aroa valley (about east-west).

The Oca-Ancón fault system is the greatest potential seismic source of northwestern Venezuela (Audemard 2000): two trenches dug across the individual active traces of the Oca and Ancón faults on segment (2) previously described revealed evidence of seismic events Ms=7.4 to 7.5 on both faults (Audemard 1996).

The recurrence of such earthquakes have been estimated in 1752 133 yr on the Ancón fault and 4300 1000 yr on the Oca fault.

San Sebastian and La Victoria

San Sebastian is a strike slip system. Almost all its extension is located offshore and is considered as the prolongation of Boconó fault into the central part of Venezuela. Probably San Sebastian concentrates the major part of Quaternary deformations and the highest seismogenic potential in central Venezuela. The maximum expected earthquake for this fault is 7.4 with a recurrence period around 400 years (González et al, 2001). La

Victoria fault extends for 350 km from Barquisimeto to Cabo Codera, and controls the beds of Aragua and Tuy rivers between La Victoria and Tejerías generating a valley with a maximum width of 1.5 km (Audemard, 2000).

La Victoria is formed by several subparallel minor faults oriented E-W. Maximum expected earthquake in this system is 6.3 with a recurrence about 545 years (Gonzáez et al, 2001).

El Pilar fault

In Northeastern Venezuela, El Pilar fault extends eastward for some 350 km, from the Cariaco trough, located south of La Tortuga island, to the Gulf of Paria, exhibiting an about 80 km long onshore portion between the gulfs of Cariaco and Paria. El Pilar fault has been subdivided in four different sections (Beltran et al, 1996):

A submarine trace west of Cumaná that bounds the Cariaco trough (pull-apart basin) on the south and ends out at the Caiguire hills, at Cumaná. A portion extending from the north side of the Caiguire hills to the Casanay-Guarapiche restraining bend. A 30 km long section that slightly diverges to the ENE and extends between Casanay an El Pilar village (Audemard, 2000).

An east-west trending portion that cuts across the swampy areas of the Sabanas de Venturini and runs offshore south of the Paria peninsula, before connecting and transferring its kinematics to the NW-SE striking Los Bajos and Soldado faults. These three faults are considered as the eastern portion of the major right-lateral strike-slip plate boundary between the Caribbean and South American plates.

El Pilar fault is the most important seismogenic source of northeastern Venezuela where the recent Cariaco earthquake (09/07/1997) with a magnitude Ms=6.8 took place. This event was associated to surface rupturing along a significant portion of the onshore

section of the right lateral El Pilar fault approximately 36 km, extending between the gulfs of Cariaco and Paria (Audemard 1999).

3. - Data and method

Earthquake focal mechanisms are widely used to estimate regional stress field. Their inversions are a useful tool to constrain tectonic stress distributions in the crust and implications on kinematics processes. Several methods exist in inverting fault plane solutions to estimate the stress field (e.g., Angelier, 1979; Gephart and Forsyth, 1984; Gephart 1990; Michael, 1984; Reaches, 1987, Rivera and Cisternas, 1990; Angelier, 2002). There are three main categories of inversion methods which are based on the following:

1) It is necessary to know which nodal plane is the fault plane a priori.

2) Use an algorithm that does not require which of the nodal planes is the fault plane.

3) Use an algorithm that can distinguish which of the nodal planes is the fault plane.

For the first category it is essential to have additional information on the fault plane such as slickenside data.

For the second category, several authors have addressed thus problem by averaging P, T and B axes to make approximate stress determinations (e.g. Isacks and Molnar, 1971, Zoback and Zoback, 1980). However, it is now widely recognized that these axes represent the moment tensor rather than the stress tensor (Mckenzie, 1969). It is however possible to infer the orientation of the principle stress axes but not the shape of the stress ellipsoid (Angelier, 1984, Angelier 2002).

For the third category, Gephart and Forsyth (1984) have proposed a method where they pick the current fault plane while inverting for the stress field by using a grid search

algorithm. However, their way of computing the misfit was modified later by Michael (1987), where a statistical approach using bootstrap resampling technique is applied.

To study variations in the stress field, confidence limits on all the quantities involved are needed. The algorithm ability to constrain confidence areas is as important as the inversion result itself. A suitable approach to deal with the confidence limits problem is to apply the bootstrap resampling technique. In this technique a random sample of fault plane solutions is selected form the original sample in such a way that some fault plane solutions will be repeated and some may be absent. Nevertheless, the distributions of error will remain the same respect to the original data. In the present study we conduct the stress inversion using the method proposed by Michael (1987)

A compilation of 125 focal mechanisms for the whole Venezuelan area made by FUNVISIS (Romero et al, 2002) is used (Table 2). The study area is from longitude 74W to 59W and latitude range from 5.5N to 13N.

Sixteen of these focal mechanisms are also present in Harvard CMT catalogue and twelve mechanisms are present in ISIC catalogue. The focal mechanism solutions are based on P-wave first motion and Table 2 indicates the parameter of the fault plane solutions. These solutions were classified in eight sub-sets of data (Table 1) to apply Michael's method (1987) according to the following criteria that keep concordance with the main Quaternary fault systems previously described:

Table 1: Different zones according to predominant fault system

Zone	Longitude W	Latitude N	Depth (km)	Geographic Context
1	73 - 59	5.5 - 13	>0	Venezuela
2	66 - 61.5	9.5 - 11.5	>0	Eastern
3	66 - 61.5	9.5 - 11.5	<= 45	Eastern Shallow
4	63.5 - 61.5	9.5 - 11.5	>45	Eastern Deep
5	68.5 - 66.0	9.5 – 11.5	>0	Central
6	73 - 68.5	6.5 - 13	>0	Western
7	73 - 68.5	10.5 - 13	>0	North West
8	73 - 68.5	6.5 – 10.5	>0	Sout West

Table 2 : Parameters of focal mechanisms compiled by FUNVISIS (Romero et al. 2002)

DATE	LATITUDE	LONGITUDE	FOCAL DEPTH	MAGNI-TUDE	NODAL PLANE A			NODAL PLANE B			T AXIS		P AXIS	
yy/mm/dd	degrees	degrees	km	mb	AZI	DIP	RAKE	AZI	DIP	RAKE	AZI	DIP	AZI	DIP
57/10/02	10.94	-62.8	60		261	90	180	351	90	0	36	0	126	0
57/10/02	10.88	-62.9	10	5.5	47	86	135	313	45.14	174.4	171	26.7	280.3	33.2
57/10/04	10.86	-62.77	6	6.7	75	45	41	196	62.4	127	59.8	60.6	316.4	7.4
57/10/06	10.88	-62.68	10		132	44	-90	312	46	-90	42	1	222	89
57/12/25	10.46	-62.55	22	5.8	215	87	100.3	321	10.8	16.3	135.7	47	305	41.1
63/07/14	10.44	-62.74	20		90	63	-123.6	214	42.1	-42.6	216.7	0.9	307.5	41.1
65/07/19	9.25	-70.44	20	5.2	55	90	180	145	90	0	190	0	280	0
66/05/14	10.38	-63.05	37		274	71	-173.9	182	84.2	-19.1	229.4	-19.1	136.5	17.5
67/01/04	10.7	-62.05	74		89	52	-136.8	329	57.4	-47	38.1	3.1	295.7	54.7
67/07/30	10.6	-67.3	14	<5.6	261	85	180	351	90	5	216.1	3.5	125.9	3.5
67/07/30	10.7	-66.95	14.1	6.5	265	69	-177.2	174	87.4	-21	221.4	12.8	127.5	16.6
67/07/30	10.18	-66.76	7.7	<5.6	50	81	173.6	141	83.7	9.1	5.7	10.8	275.3	1.9
67/07/30	10.95	-66.88	21	<5.6	276	59	128.4	39	47.8	44	239.9	57	339.8	6.4
67/12/21	7	-72	29	4	138	76	0	48	90	166	2.1	9.8	93.9	9.8
68/03/12	13.15	-72.3	58	5.3	64	28	90	244	62	90	154	73	334	17
68/05/13	9.06	-71.1	29	4.9	228	60	130.9	348	49.1	41.4	191.3	54.7	290.2	6.3
68/09/20	10.76	-62.7	103	6.2	226	15	66.7	70	76.2	96	348.2	58.3	155	31
68/11/17	9.6	-72.6	150	5.8	149	8	179	240	89.9	82	142.1	44.6	337.9	44.3
69/10/20	10.9	-72.4	36	5.7	47	50	-52.4	170	65	-136.6	270	9	23	49
69/10/20	10.87	-72.49	36	5.7	2.9	72.3	0	92.9	90	-162.3	226.5	12.4	319.3	12.4
70/01/27	7.49	-72.09	31	5.6	240	60	-143.9	130	59.4	-35.5	4.9	0.4	95.3	45.6
70/05/19	10.9	-68.9	15	5.1	5	70	-38.1	110	54.6	-155.2	60.6	9.7	322.2	40.7
70/12/14	9.9	-72.68	158	5.1	159	14	-122.2	12	78.2	-82.4	95.6	32.8	291.6	56.2
73/07/08	6.8	-73	156	5.4	44	64	154.1	146	66.9	28.5	5.8	36	274.5	1.9
74/06/12	10.61	-63.47	0	5.7	213	70	-31.9	315	60.3	-156.8	265.8	6.3	171.2	36.3
75/03/05	9.13	-69.87	25	5.6	210	50	56.4	76	50	123.4	52.6	64.9	143.1	0.2

Table 2 (continued)

DATE	LATITUDE	LONGITUDE	FOCAL DEPTH	MAGNI-TUDE	NODAL PLANE A			NODAL PLANE B			T AXIS		P AXIS	
yy/mm/dd	degrees	degrees	km	mb	AZI	DIP	RAKE	AZI	DIP	RAKE	AZI	DIP	AZI	DIP
75/04/05	10.1	-69.6	36	5.5	112	80	168.6	204	78.8	10.2	67.9	15.1	158.1	0.8
75/04/05	9.56	-69.52	2	5.5	294	68	0	204	90	158	156.8	15.4	251.2	15.4
77/10/04	10.16	-61.99	21	5.1	273	52	-161	171	75.1	-39.6	226.7	14.7	124.8	38.1
77/12/11	9.56	-69.52	2	5.5	70	65	139.3	180	53.7	31.6	30.2	45.8	127.3	6.9
79//05/05	9.09	-71.56	22	5.6	119	53	5	26	86	142.9	335.8	28.3	78.5	22.1
79/06/C**	10.45	-63.6	<5.1		177	85	-11.3	268	78.7	-174.9	222.9	4	132	11.5
79/06/C**	10.4	-63.6	<5.1		337	75	-161.3	242	72	-15.8	109.1	2	200	23.7
79/07/ C**	10.5	-63.25	<5.1		250	85	-141.3	156	51.4	-6.4	16.6	22.3	120.4	30.2
79/07/ C**	10.45	-63.17	<0.1		58	10	180	148	90	80	48.1	44.1	247.9	44.1
80/01/02/C**	8.71	-71.08			29	65	103.2	180	28.1	63.9	323.7	67.3	109.2	19
80/01/02/C**	8.66	-71.03			221	30	-106.6	60	61.4	-80.6	143.1	15.9	351.9	72
80/11/26	7.96	-72.62	40	5.2	57	64	170.9	151	81.9	26.3	17	24.2	281.4	12.1
82/05/10	10.5	-62.56	79.8	5.3	204	9	-4	298	89.4	-99	36.8	43.7	199	44.9
82/07/04	7..65	-72.19	53.5	5.5	136	66	4.9	44	85.5	155.9	357.4	20.1	92.4	13.4
83/03/08	10.89	-62.03	85	5.9	260	7	119.8	50	83.9	86.5	316.1	51	143.2	38.8
83/04/11	10.08	-62.61	19.2	6	3	43	-57.6	142	54.9	-116.6	250.6	6.3	356.1	61.5
84/C **	8.4	-70.9	<02	<4	45	44	77.6	242	47.3	101.7	222.9	81.3	323.7	1.7
84/02/11	12.08	-60	39.1	5.3	348	53	-142.2	233	61	-43.6	292	4	195.5	50.5
84/06/14	10.05	-69.78	18	5.2	340	65	-11.7	75	79.4	-154.5	205.4	9.7	300	25.4
84/08/20	10.62	-62.53	21.8	5.1	80	71	165	175	75	19.6	38.3	23. 8	306.8	3.3
84/10/05	11.34	-60.25	41.2	4.4	172	57	-150.7	65	65.8	-36.7	120	5	25	43
85/87/90C**	9.9	-68.7	<51	3 - 3.9	168	84	0	78	90	174	32	4.2	123.2	4.2
85/87/94C**	10.7	-67	<51	3 - 3.9	355	60	0	85	90	-150	215.9	20.7	314.1	20.7
85/11/28	11.76	-61.36	49	5.2	201	27	123.9	344	68	74.1	227	64	86	21
86/C**	10.2	-67	<51	3.0 - 5.8	48	65	-7.1	141	83.6	-25.2	272	12.7	7.3	22.2
86/C **	9.5	-69.2	<02	3.0 - 4.0	315	60	0	225	90	150	175.9	20.7	274.1	20.7

Table 2 (continued)

DATE	LATITUDE	LONGITUDE	FOCAL DEPTH	MAGNI-TUDE	NODAL PLANE A			NODAL PLANE B			T AXIS		P AXIS	
yy/mm/dd	degrees	degrees	km	mb	AZI	DIP	RAKE	AZI	DIP	RAKE	AZI	DIP	AZI	DIP
86/C **	9.2	-69.9	<02	<0.4	190	40	52.5	55	59.3	117	13.3	64.5	125.9	10.4
88/89/90C**	10.3	-67	<51	3.0 - 4.0	39	75	-31.5	138	59.7	-162.6	91.2	10	351.8	32.7
86/06/11	10.7	-62.93	20	6	97	52	-159.4	354	73.9	-39.8	50	13.9	308.4	39.1
86/07/18	10.8	-69.35	15	5.6	64	41	106.2	223	51	76.4	78	78	323	5
86/07/18C**	10.8	-69.36	44.9	5.6	204	85	21.8	112	678.3	174.6	70.1	78.9	336.1	11.6
86/09/12C**	11.04	-69.44	8.2	4.4	65	53	144.8	178	62.6	42.7	36.1	48.7	299.5	5.7
87/06/01	12.24	-61.54	156	4	62	36	177.5	154	89	54	33	36	274	34
88/C **	10.3	-69.8	<02	<0.4	325	55	180	55	90	145	184	24	286	24
88/03/10	10.16	-60.13	54	7	256	38	-67.3	48	56	-106.8	150	9	274	73
88/0311	10.06	-60.32	47	4.5	213	38	-131.2	81	63	-62.8	152	14	35	62
88/03/12	10.19	-60.2	33	5.3	42	31	-132.6	269	68	-67.9	343	20	213	61
88/03/16	9.72	-60.47	55	5.2	40	45	-118.1	257	51	-64.8	330	3	230	70
88/03/25	10.04	-60.26	56	4.9	16	63	-173.4	283	85	-27.2	333	15	236	23
88//04/12	10.35	-63	53.9	5.5	66	45	136.4	190	60.8	54.1	49.2	57.7	301.8	8.9
88/06/24	10.28	-60.25	53	4.9	238	44	-89.3	59	46	-90.7	148	1	328.9	89
88/07/12	11.04	-62.96	15	5.1	104	50	-166.2	5	79.4	-40	60.5	19	316.2	35.7
89/01/30	7.8	-72.17	11.2	4.4	46	50	58.2	270	49.4	122.2	157.9	0.3	248.6	66.2
89/04/15	8.5	-60.32	18.5	5.8	194	29	-153	80	77.3	-63.7	149.3	27.6	19.6	50.7
89/04/30	11.1	-68.18	11.1	5.7	167.9	62.7	-177.3	259.2	87.6	-27.3	126.3	18.9	28.5	18.9
89/04/30	11.1	-68.18	11.1	5.7	178.1	52.9	-170.6	273.8	82.5	-37.5	139.5	25.2	36.7	25.2
89/04/30	11.1	-68.18	11.1	5.7	167.2	67.8	-158	265.9	69.7	-23.8	123.8	13.7	29.5	17.3
89/05/04	11.14	-68.21	13.6	5	137.2	74.2	-168.7	230.3	79.1	-16.1	93.3	11.1	1.1	11.1
89/05/04	11.14	-68.21	13.6	5	163.5	54.8	-86	336.5	35.4	-95.7	250.6	9.7	89.8	79.7
90/C**	10.8	-65.5	<51	3-5.8	81	70	180	171	90	20	37.8	14	304.2	14
90/03/21	10.72	-65.36	32.4	5.2	109	62	-36.3	218	58.5	-146.6	72.1	44	164.2	21
91/08/07	9.99	-69.992	18.2	5	45	70	-141.9	300	54.6	-24.8	169.4	9.7	267.8	40.7

Table 2 (continued)

DATE	LATITUDE	LONGITUDE	FOCAL DEPTH	MAGNI-TUDE	NODAL PLANE A			NODAL PLANE B			T AXIS		P AXIS	
yy/mm/dd	degrees	degrees	km	mb	AZI	DIP	RAKE	AZI	DIP	RAKE	AZI	DIP	AZI	DIP
91/08/17	10.003	-70.032	16.2	5.3	310	45	-35.8	67	65.6	-129.1	184.1	12	290.1	52.4
91/08/17	9.74	-69.83	15	5.5	344	86	0	74	90	-176	200.9	2.8	299.1	2.8
91/08/17	10.54	-62.2	45.2	5.3	124	14	-48.9	262	79.5	-99.3	359.9	33.9	160.6	51.6
91/08/20	10.05	-70.1	1.8	4.5	19	68	174.7	111	85.1	22.1	337.1	19	243	11.8
91/08/20	10.054	-70.105	1.8	4.5	331	42	-18.5	75	77.7	-130.5	194.7	22	306.5	42.5
91/08/20	9.988	-70.014	18	4.2	345	40	-10.4	83	83.3	-129.5	203.5	27.4	317.8	38.6
91/08/21	10.038	-70.032	15.1	4.5	75	75	-126.9	326	39.5	-24	192.1	21.3	306.6	46.8
91/08/21	10.03	-70.03	15.1	4.5	30	55	-20.3	132	73.5	-143.2	256.4	11.8	356.5	37.4
91/09/02	10.063	-70.032	7.9	4.7	0	45	12.6	261	81.1	134.3	209.5	37.5	318.6	23
91/09/14	10.021	-70.041	9.3	4.1	280	65	123.1	43	40.6	40.5	234.7	56.7	346.6	13.8
91/09/14	10.02	-70.41	41	4.1	37	66	-6	130	84.8	-149	259.7	16.8	357.7	24.7
94/05/31	7.423	-72.001	13.5	6.1	63	75	-128.5	315	40.9	-23.3	181.1	20.6	293.8	45.8
94/11/09	7.53	-71.73	21.3	5.2	178	42	112.4	329	51.8	71.1	100.7	74.4	72.3	5
95/C**	10.2	-67.9	<51	3-4.0	0	80	16	267	73.5	169.6	224.3	18.9	132.8	4.5
95/12/29	9.99	-70.08	16.2	5.1	47	65	103.7	197	28.3	63.1	342.6	67.1	126.8	18.9
95/12/29	9.99	-70.08	16.2	5.1	47	65	155.3	148	67.7	27.2	8.2	34.5	277	1.8
95/12/31	9.86	-69.91	15	5.1	257	74	-176.4	166	86.5	-16	212.6	8.7	120.4	13.8
97/04/15	10.69	-69.63	15	5.2	109	65	163.8	206	75.4	25.9	69.6	28.5	335.8	6.9
97/07/09	10.545	-63.515	9.41	6.9	270	75	-136.1	166	47.9	-20.4	32.2	16.9	137.5	41.1
00/10/04	11.016	-62.3	119	6	90	58	78.5	291	33.8	107.7	328.8	74.2	188.3	12.3
01/10/31	10.729	-67.016	6.6	3.8	55	45	20.8	311	76.6	131.1	261	42.6	9.3	18.8
02/04/01	10.095	-69.07	0	3.4	3	49	9.1	267	83.1	138.6	216.4	33.3	322	22.3
02/04/12	9.609	-69.996	18.5	4.4	60	70	0	330	90	-20	16.8	14	283.2	14
02/04/14	10.158	-67.919	5.5	3.5	262	71	-146.9	160	58.9	-22.4	28.7	7.8	124.5	36.6
02/04/18	12.033	-69.459	30.2	4.2	28	47	0	298	90	137	244.2	28.8	351.8	28.8
02/04/18	10.199	-64.91	0	4	30	40	35.9	271	67.9	124.2	223.4	53.9	336.6	16

C**: Composite focal mechanism

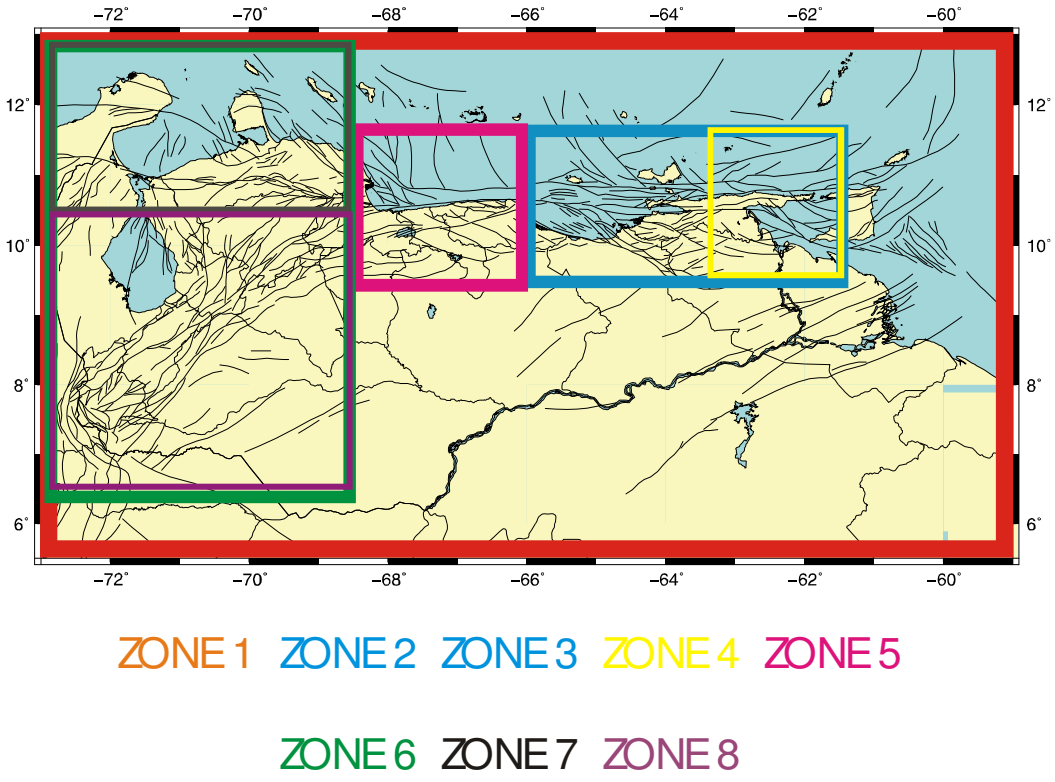

Figure 5: Eight different areas according to a predominant fault system. Eastern region has been subdivide in two areas of shallow seismicity and a deep seismicity towards north east.

To analyze the data, we used the software for analyses of seismicity patterns, ZMAP (version 6.0) (Wiemer 2001). The code developed by Andy Michael (1984) runs under ZMAP, and requires the input data organized as follows: longitude, latitude, year, month, day, magnitude, depth, hour, minute, dip direction, dip, rake and solution uncertainty.

4.-Results

The regional variation of the stress tensor is analysed using the inversion results from focal mechanisms. In doing this, we have divided the area into eight zones which are

identified based on the general trends of the active faults in the entire Venezuela region (See Figures 4 and 5).

Solution for the overall zone 1, which includes 125 fault plane solutions, is shown in figure 6. A predominant strike slip regime is evidenced in the solution with a configuration $S_H > S_V > S_h$.

Solution shown in Figure 6 seems to be the most stable solution since it uses all 125 fault plane solutions. The resulting orientation of the stress tensor indicate strike slip faulting regime when σ_1 lies almost horizontally in the NW-SE orientation and σ_2 is near vertical. This data set in zone 1 represents the transcurrent deformation in Venezuela.

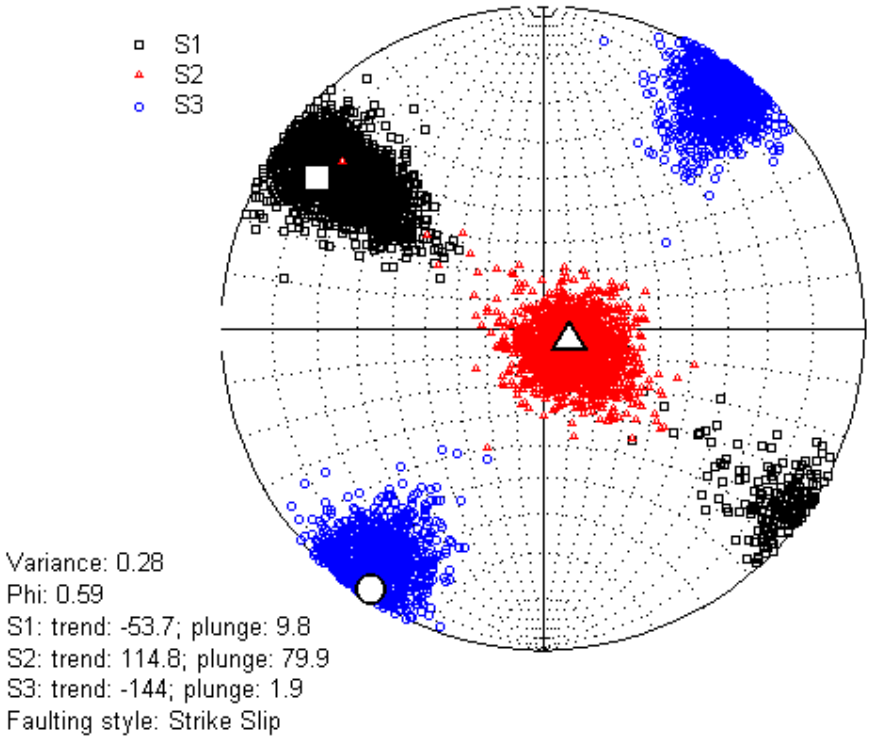

Figure 6: Stress inversion for Venezuela, zone 1. Solution obtained with 125 focal mechanisms

From figure 6 to Figure 14: square=σ_1, triangle=σ_2 and circle=σ_3

Figures from 7 to 13 show the spatial distribution of the focal mechanism according to the selected zone while Table 3 summarizes the parameters of the stress tensors deduced form the inversion of focal mechanisms according to Michael's method.

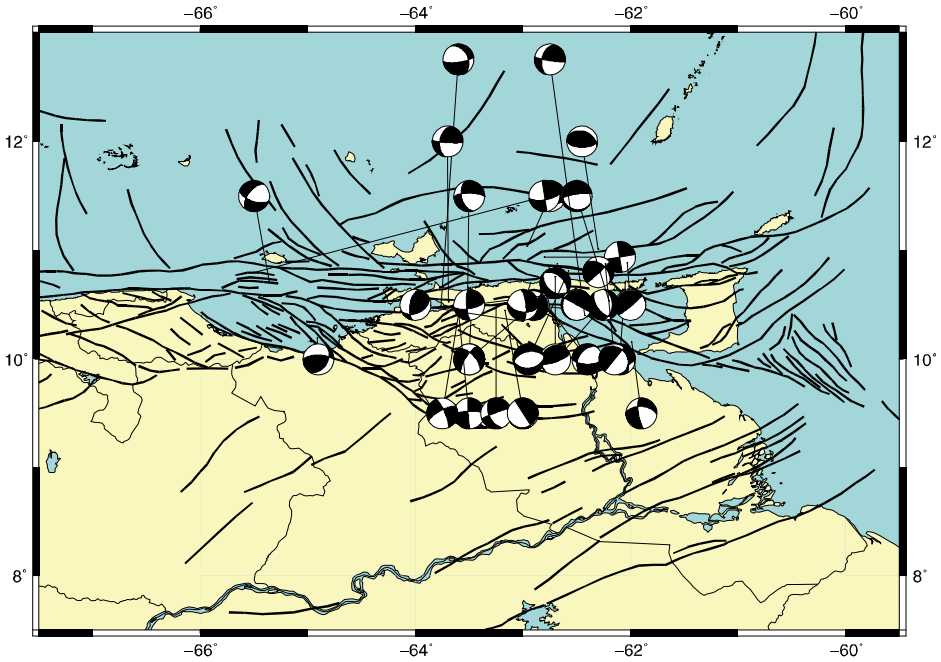

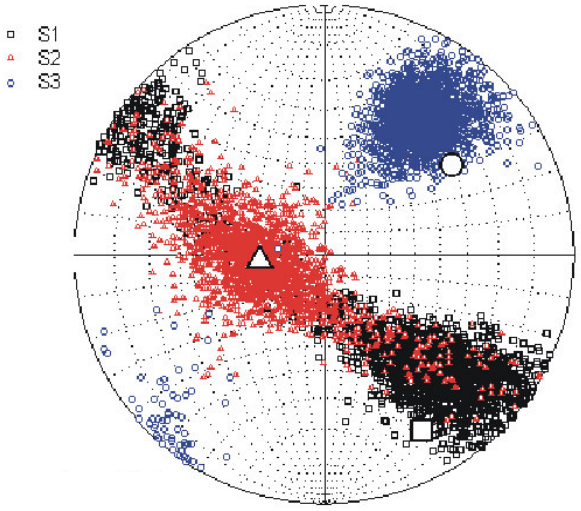

Figure 7: Stress Inversion Eastern Venezuela: zone 2.

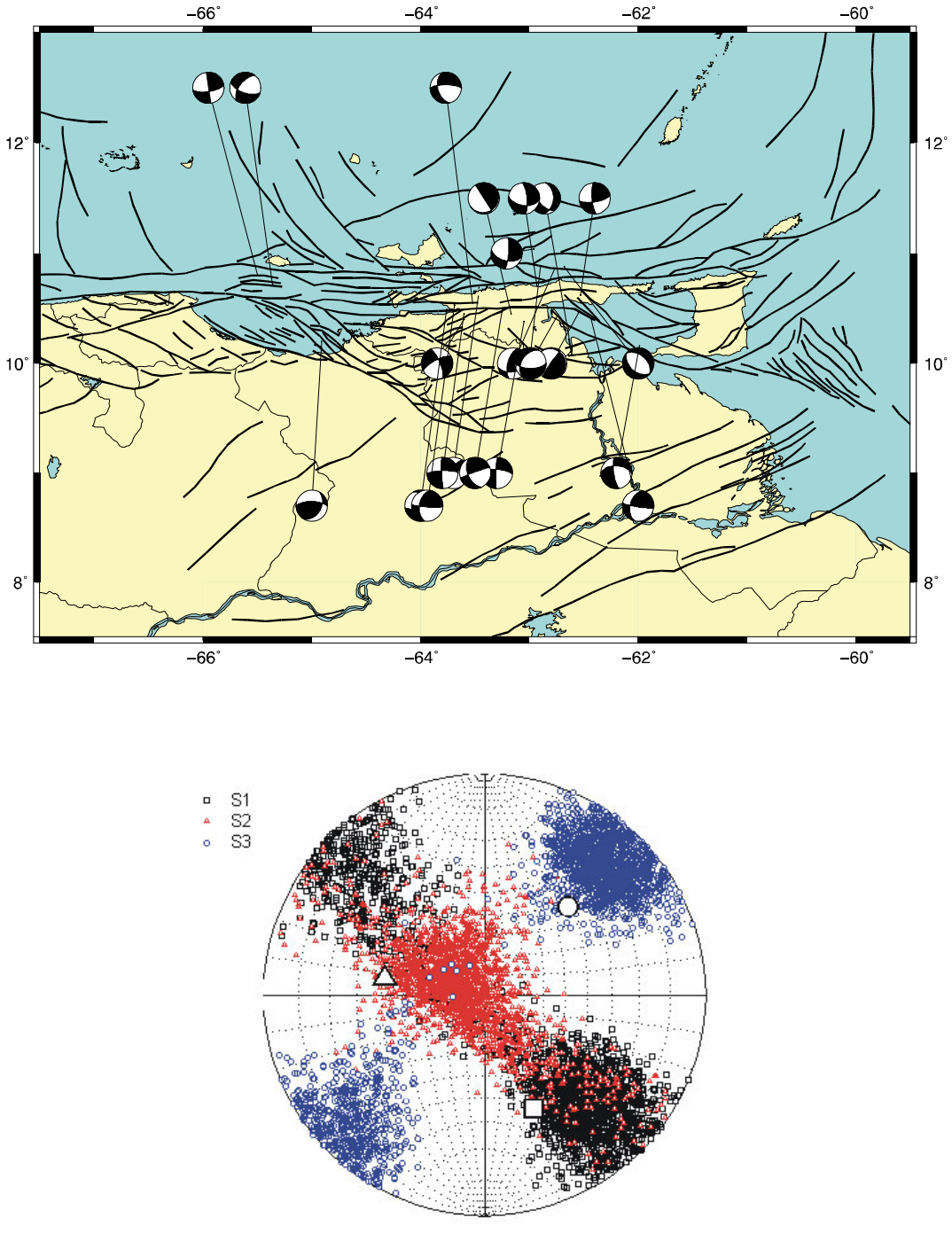

Figure 8: Stress Inversion for Eastern Venezuela. Shallow seismicity: zone 3.

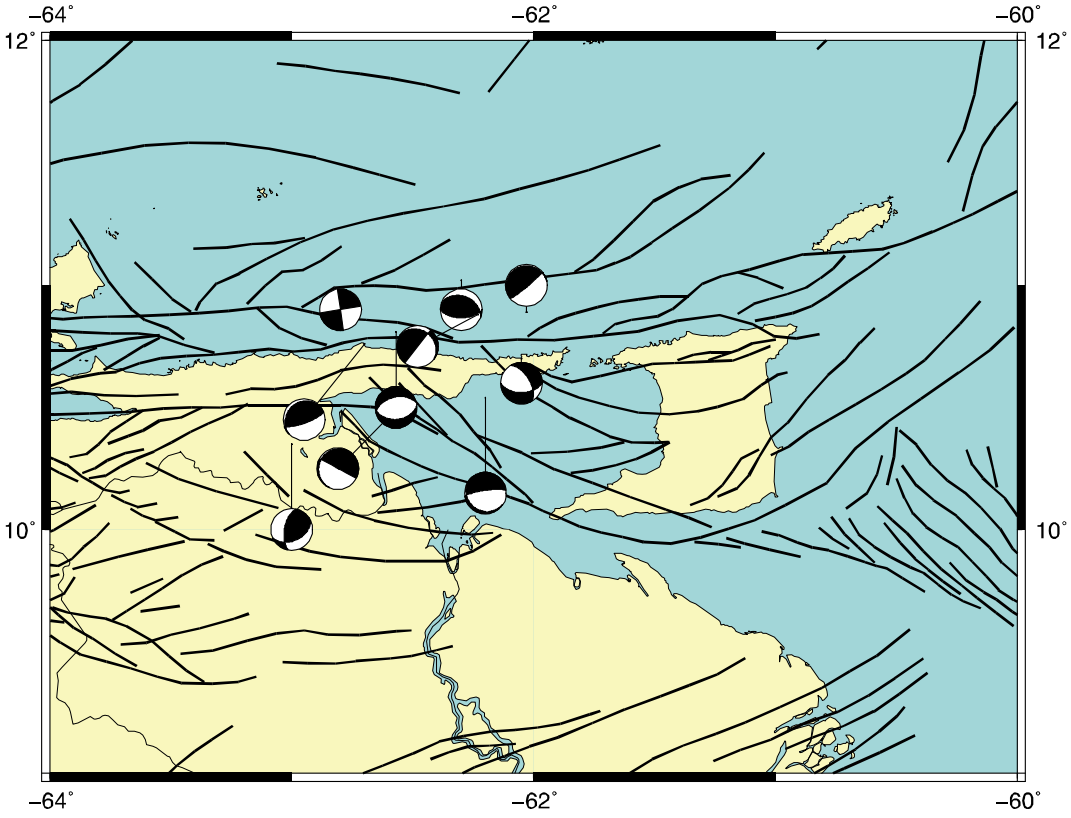

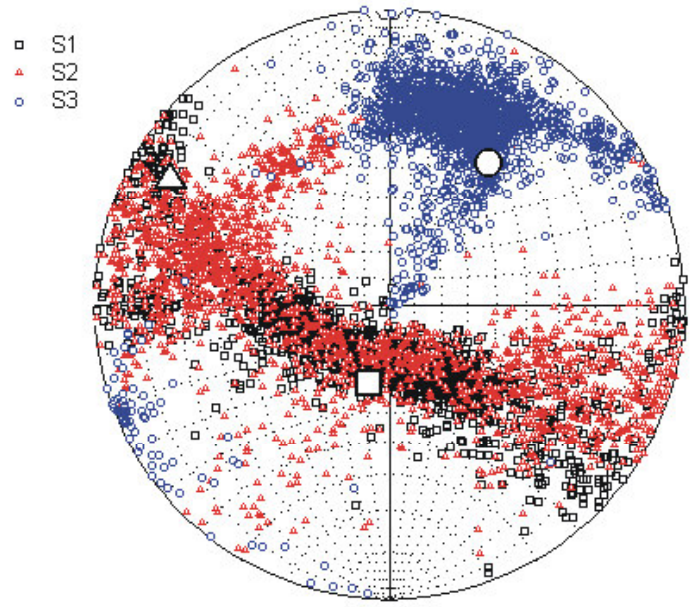

Figure 9: Stress Inversion for Eastern Venezuela. Deep seismicity: zone 4.

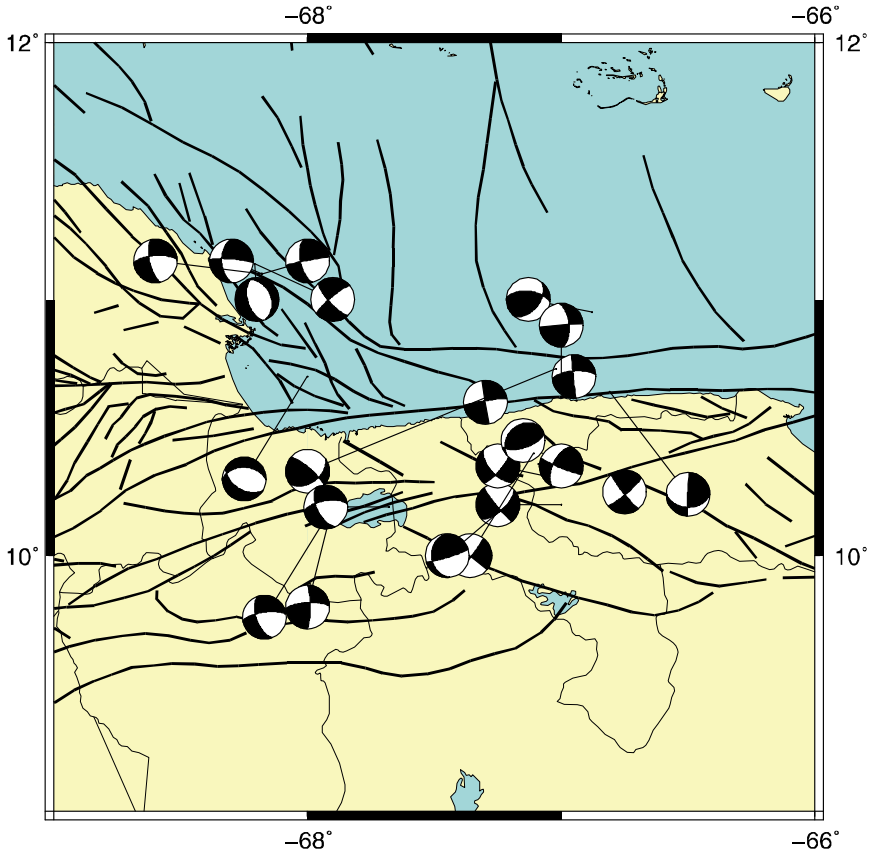

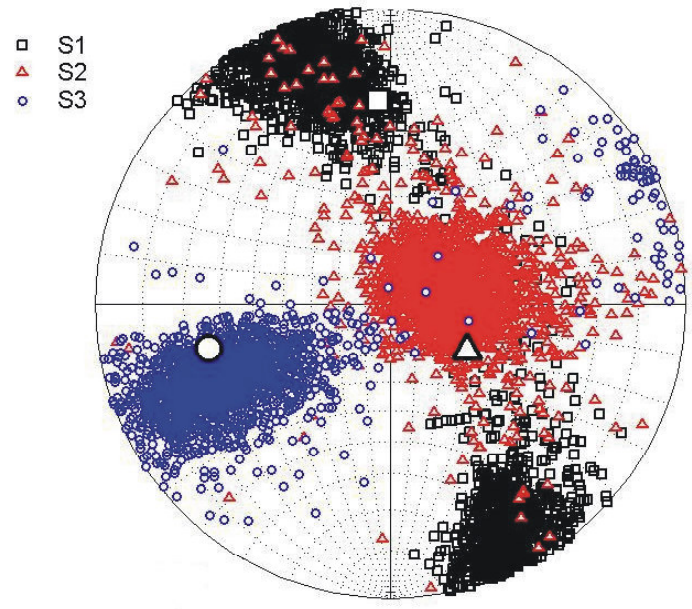

Figure 10: Stress Inversion for Central Venezuela: zone 5.

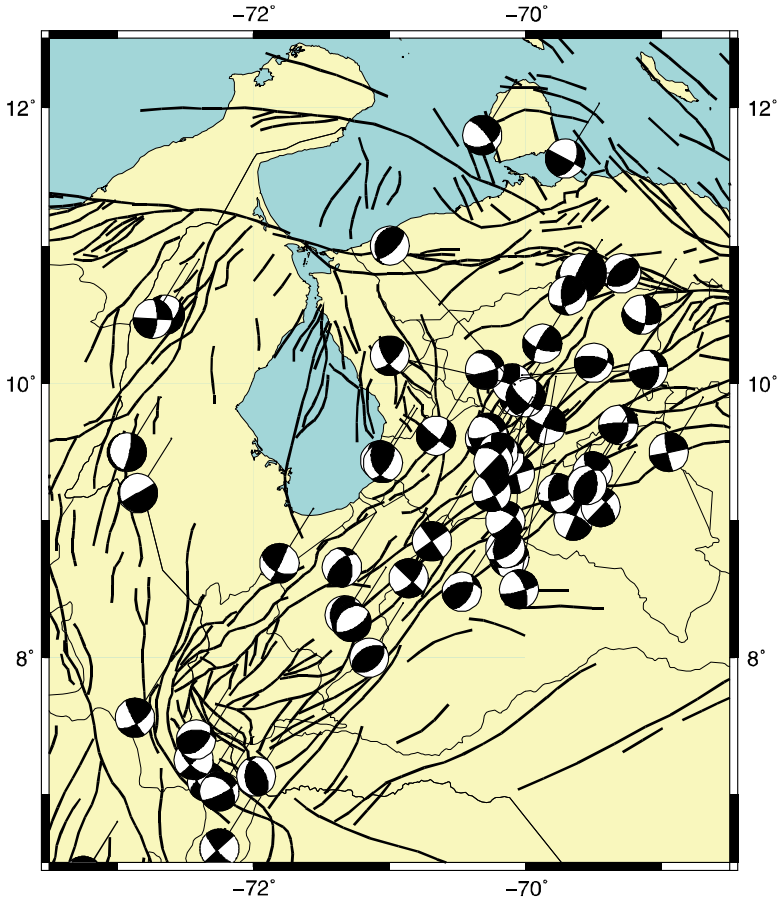

Figure 11: Stress Inversion for Western Venezuela: zone 6.

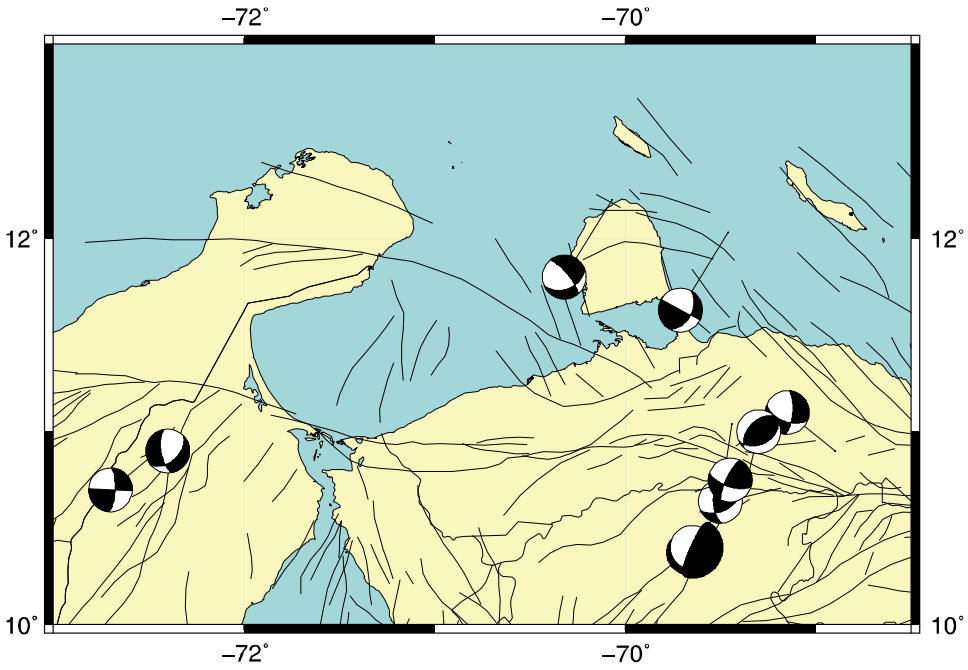

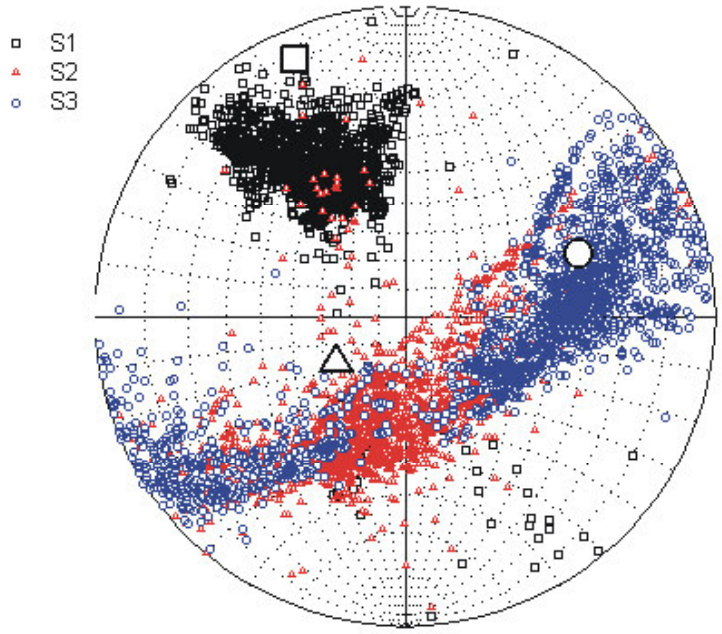

Figure 12: Stress Inversion for North West Venezuela: zone 7

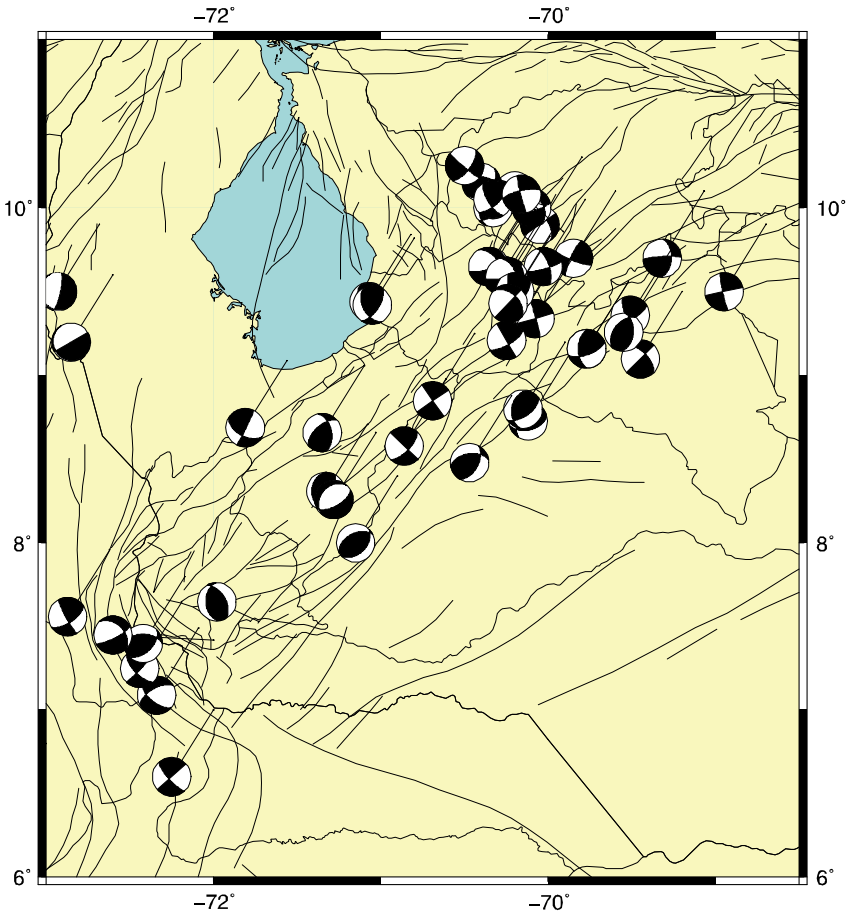

Figure 13: Stress Inversion for South West Venezuela: zone 8.

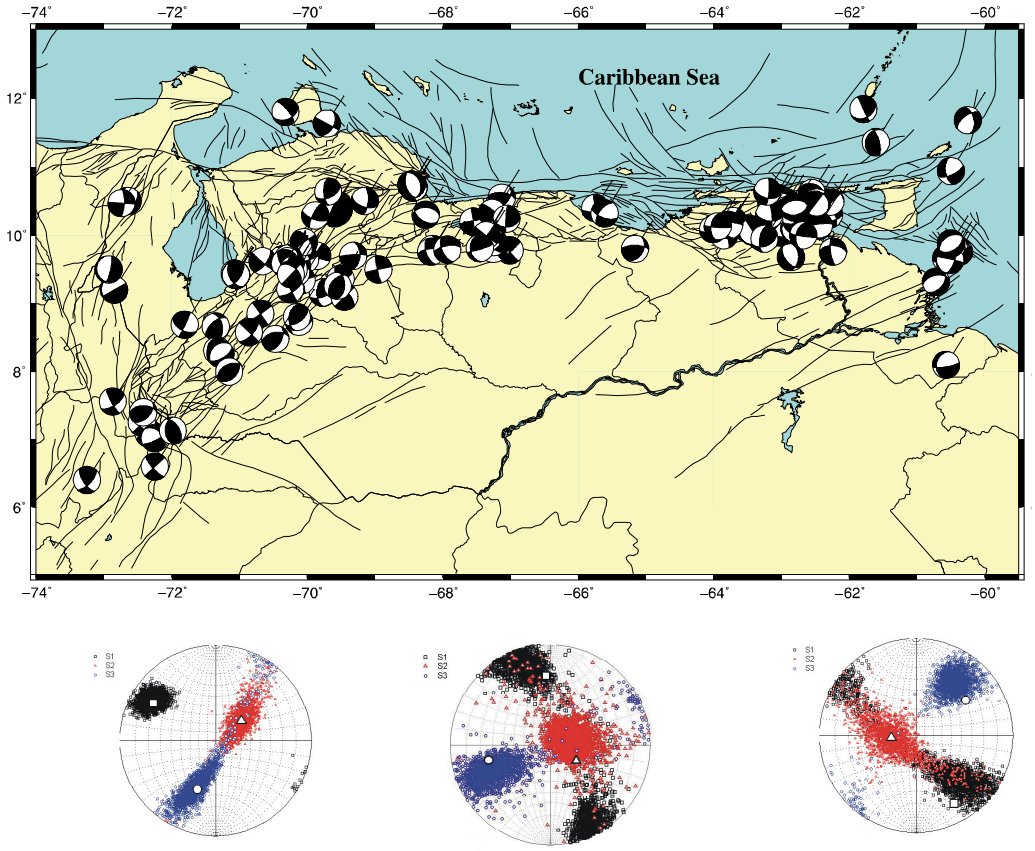

Figure 14: Venezuela stress inversion. Three solutions are shown to illustrate the stress solutions in western, central and eastern Venezuela.

A distribution of 33 focal mechanisms in zone 2 as well as the stress inversion is shown in Figure 7. The entire eastern area is characterized by presenting mainly crustal earthquakes and a minor sample of deeper events presumably associated with the subduction occurring in the north west part of zone 2. The fault plane solutions corresponding crustal earthquakes are mainly located along El Pilar fault system and are essentially strike slip faulting type. The solution in zone 2 is not as well constrained as in zone 1. Nevertheless, zone 2 complies with dominant strike slip and the solution shows NW-SW compression.

Zone 3 with 23 focal mechanisms shows basically the same tendency as zone 2. There are not significant differences between zone 2 and zone 3. This suggests that solution in

zone 2 is strongly influence by the sample of crustal events. Thus, zone 2 shows to be a reliable solution.

Zone 4 counts with only 10 events. This affect the homogeneous distribution of the stress and therefore the solution is not reliable in terms of well defined constrained areas since the spread is wider than in zone 3. Another notable difference is the direction of σ_1 which turns to be vertical and σ_2 is close to be horizontal defining in such a way, a plane of rotation that is consistent with subduction towards north east where forces of slab pull and sinking plate are present.

Zone 5 is the zone with less fault plane solutions regarding the main division of Venezuela in three areas. This zone presents a more uniform distribution in the inversion solution than zone 4. The faulting style is strike slip with a change in the orientation of σ_1 respect to zone 3. Thus, σ_1 is oriented towards north and the general trend for the most compressional principal stress becomes more N-S oriented. In zone 5, San Sebastián and la Victoria fault play a key role in the seismotectonics of the region. In the Central region of Venezuela, some normal mechanisms are identified offshore. These focal mechanisms were subtracted from the initial data base to apply the inversion method, under the assumption that they actually belong to a different tectonic structure rather than to be involved in the kinematics process of the general strike slip tendency of the overall transcurrent system.

Zone 6 has 58 focal mechanisms. This zone exhibits a remarkable well constrained and homogeneous solution of the stress tensor respect to other zones. The direction of σ_1 is WNW-ESE. This area presents a more complex faulting regime since in the sample there is a significant presence of thrust faulting earthquakes among the focal mechanisms.

Zone 7 with only 10 events is badly resolved. As well as zone 4, there are not enough focal mechanisms to achieve a reliable solution since presents a wide spreading area due to few input data. The orientation of the stress tensor describes a trend NW-SE. It is observable a rotation of the compressive stress in comparison with zones 6 and 7 and presents a general strike slip regime. The predominant fault system in the area is Oca-Ancón.

Zone 8 counts with 49 fault plane solutions making the result of the inversion well constraint as in zone 6. Both solutions, zone 6 and 8, are very similar, indicating the primacy of the sample 8 over the few events in zone 7 in the inversion of zone 6. The principal stress σ_1 becomes more horizontal and σ_3 more oblique. The direction of the stress tensor indicates a WNW-ESE orientation. The predominant fault system in the area is Boconó.

Table 3: Stress inversion results for eight zones in Venezuela by using Michael's method

Definition: $\phi = \frac{\sigma_2 - \sigma_3}{\sigma_1 - \sigma_3}$ Where σ_1: most compressional principal stress, σ_2: intermediate principal stress and σ_3: most extensional principal stress (Michael, 1987).

				σ_1		σ_2		σ_3	
Zone	Number of focal mechanisms	Variance	ϕ	Azimuth	Plunge	Azimuth	Plunge	Azimuth	Plunge
1	125	0.28	0.59	306.3	9.8	114.8	79.9	216	1.9
2	33	0.24	0.62	135.3	30.1	288.2	56.8	37.9	12.5
3	23	0.23	0.68	134.9	29.2	311.8	60.7	44.2	1.4
4	10	0.15	0.55	275.4	2	179.1	71.4	6	18.4
5	22	0.26	0.54	339.4	10.9	92	63.4	244.6	23.9
6	58	0.23	0.23	302.3	16.1	62.4	60	204.8	24.5
7	9	0.15	0.51	330.2	28.4	180.5	57.9	67.7	13.6
8	49	0.21	0.28	296.4	14.1	50.4	58.3	198.8	27.7

Even though most of the earthquakes are shallow, the eastern part of Venezuela has a seismicity that corresponds to subduction events and crustal events, which explains the discrimination for deeper and shallow events in the eastern part of Venezuela.

The variance for the different samples ranges form 0.15 to 0.28. Inversions in zones 1, 5 and 6 show a relative good fit to homogeneous stress field. A particular case is the difference due to depth between zones 3 and 4 which indicates crustal and deeper seismicity that reflects the subduction interaction between the Caribbean and South America, leading to a change in the plane of main stresses where a predominant normal mechanism appears. However, since the number of focal mechanism is small, there is a poor resolution of the area and therefore a poor fit to a homogeneous stress field from deep seismic events.

5. - Discussion and conclusions

The variation in the stress field along the Venezuelan region from East to West is studied using the stress inversion from focal mechanisms of earthquakes.

The entire data set of 125 events are distributed along different segments of mainly three fault systems; (1) Eastern, (2) Central and (3) Western.

Although the inversion of the entire data set (all 125 events) represents a clear strike slip faulting regime with σ_1 oriented almost horizontally in the NW-SE direction, there are significant variations locally among the three major fault systems.

Figure 14 summarizes the stress inversion results for these three fault systems from East to West as represented by: (1) El Pilar fault system, (2) San Sebastián and La Victoria fault systems and (3) Boconó fault system.

In all three cases the dominant faulting regime is strike slip ($S_H > S_V > S_h$). However, both the orientation of σ_1 and its plunge varies from east (plunging SE with a NW-SE azimuth) to central parts (plunging N, with N-S azimuth) and finally to the west (plunging NW with a WW-SE azimuth).

The stress tensor in the east is complicated by the influence of the deep subduction process occurring along the Lesser Antilles. The difference in the stress tensor from the shallow and deep events indicates clearly this observation (zones 2 and 3).

In the Central part, the two dominant fault systems (i.e. San Sebastián and La Victoria faults) give rise to the slight rotation of the stress tensor more towards North.

In the western part, the marked change in the general azimuth trend of the faults in the Boconó fault system (from E-W to WE-SW) almost 45°, indicates a change also in the stress tensor in this area where the σ_1 becomes more oriented in the NW-SE azimuth plunging more towards NW.

This observation is concordant with what might be expected in an area where subduction processes become important. The influence of NW dipping subduction in the East is the change of plunge of σ_1 towards SE. The opposite effect on the western part is the change of plunge of σ_1 towards NW which is probably associated with the influence of subduction dipping east.

The results presented in this study demonstrates the remarkable correlation of the regime stress tensor controlled by the general plate motions and the associated deformation in a transcurrent setting where the entire Venezuela area accommodates the lateral transition from westerly dipping subduction in the North west to the easterly dipping subduction in the south west through predominantly strike slip faulting along the three main systems, El Pilar fault system in the East, San Sebastián and La Victoria fault systems in the central area and Boconó fault system in the west.

References

Angelier, J.,1979 Determination of the mean principal direction of stress for a given fault population, Tectonophysics 56, T17-T26.

Angelier, J., 1984. Tectonic analysis of fault slip data sets, J. Geophys. Res. 89, 5835-5848.

Angelier, J., 2002. Inversion of earthquake focal mechanisms to obtain the seismotectonics stress: IV. A new method free of choice among nodal planes. Geophys. J. Int. 150, 588-609.

Audemard, F.A., Giraldo, C., 1997. despalzamientos dextrales a lo largo de la frontera meridional de la placa Caribe, Venezuela septentrional. VII Cong. Geol. Venezolano, Porlamar 1, 101-108.

Audemard, F., 1996. Paleoseismicity studies on the Oca-Ancón fault system, northwestern Venezuela. Tectonophysics 259, 97-80

Audemard, F., 1999. El sismo de Cariaco del 09 de julio de 1997, edo. Sucre, Venezuela: nucleación y progresión de la ruptura a partir de observaciones geológicas. VI Cong. Venezolano de Sismol. e Ing. Sísmica, Mérida (in CD-Rom) .

Audemard, F.A., 2000. Major active faults of Venezuela. Proceedings 31st International Geological Congress, Rio de Janeiro, Brasil, 4 pp. (extended abstract in CD-Rom).

Audemard, F.E., Audemard, F.A., 2002. Structure of the Mérida Andes, Venezuela relations with the South America-Caribbean geodynamic interaction. Tectonophysics 345, 299-327.

Audemard, F., Romero, G., Rendon, H., Cano, V., 2005. Quaternary fault kinematics and stress tensors along the southern Caribbean from fault-slip data and focal mechanism solutions. Earth Science Reviews 69, 181-233.

Beltrán, C., 1993. Mapa Neotectonico de Venezuela. FUNVISIS. Departamento de Ciencias de la Tierra.

Beltrán, C., Rodríguez, J.A., Singer, A., 1996. The El Pilar Fautl active trace (Northeastern Venezuela): neotectonic evidences and paleoseismic data. III ISAG, Saint-Malo, France. 152-156.

Casas, A., 1991. Estudio Sismotectónico del valle del Yaracuy. FUNVISIS-Univ. Of Zaragoza, Unpubl. Rpt.

Corredor, F., 2003. Seismic strain rates and distributed continental deformation in the northern Andes and the three-dimensional seismotectonics of northwestern South America. Tectonophysics 372, 147-166.

Cortés, M., Angelier, J., 2005. Current states in the northern Andes as indicated by focal mechanisms of earthquakes. Tectonophysics. In Press.

Ferrer, C., 1991. Características geomorfológicas y geotectónicas de un segmento de falla de Boconó entre la ciudad de Mérida y la laguna de Mucubají, Estado Mérida. Guía de la excursión. Esc. Latinoamericana de Geof., 25 pp.

Freymuller, J.T., Kellog, J.N., Vega, V., 1993. Plate motions in the north Andean region. J. Geophys. Res. 98, 21853-21863

Gephart, J.W., Forsyth, D.W., 1984. An improved method for determining the regional stress tensor using earthquake focal mechanism data: Application to the San Fernando earthquake secuence, J. Geophys. Res. 89, 9305 -9320.

Gephart, J.W., 1990. FMSI: A FORTRAN program for inverting fault/slickenside and earthquake focal mechanism data to obtain the original stress tensor, Comut. Geosci., 16, 953-989.

Giraldo, C., 1989. Valor del desplazamiento dextral acumulado a lo largo de la falla de Boconó, Andes venezolanos. GEOS 29, 186-194.

Giunta, G., Beccaluva, L., Coltorti, M., Siena, F., Vaccaro, C., 2002. The southern margin of the Caribbean Plate in Venezuela: tectono-magmatic setting of the ophiolitic units and kinematic evolution. Lithos 63 19-40.

González, J., Molina, A., Cedeño, F., Audemard, F., 2001. Evaluación de la amenaza sísmica del estado Vargas y algunas localidades de la Zona Metropolitana. Serie Técnica del taller: Estudios de métodos y acciones para contrarestar los efectos producidos por terremotos en Caracas (1999-2001) 1, 74-83.

Grandison, M., Atakan, K., 2005. Seismotectonics of Jamaica. Geophys. J.Int. 160, 573-580.

Isacks, B.L., Molnar, P., 1971. Distribution of stresses in the descending lithosphere form a global survey of focal mechanism solutions of mantle earthquakes, Rev. Geophys., 9, 103-174.

Leroy, S., Maufret, A., 1996. Intraplate Deformation in the Caribbean region. J.Geodynamics 21, 113-122.

Mckenzie, D.P., 1969. The relation between fault plane solutions for earthquakes and the directions of principal stresses. Bull. Seismol. Soc. Am. 59, 591-601.

Michael, A.J., 1984. Determination of stress from slip data: faults and folds, Journal of Geophysical Research, 89, 11517-11526

Michael, A.J., 1987. Use of focal mechanisms to determine stress: a control study, Journal of Geophysical Research 92, 357 -368.

Moreno, B., Grandison, M., Atakan, K., 2002. Crustal velocity model along the southern Cuban margin: implications for the tectonic regime at an active plate boundary, Geophys. J.Int. 151, 632-645.

Reaches, Z., 1987. Determination of the tectonic stress tensor slip along faults that obey the Coulomb yield condition. Tectonics 6, 849-861.

Rivera, L., Cisternas, A., 1990. Stress tensor and fault plane solution for a population of earthquakes. Bull. Seismol. Soc. Am. 80(3), 600-614.

Romero, G., Audemard, F., Rendón, H., Orihuela, N., 2002. Compilación de soluciones focales para sismos sentidos en Venezuela y áreas vecinas 1957 – 2002. FUNVISIS map.

Singer, A., Beltrán, C., 1996. Active faulting in the Southern Venezuelan Andes and Colombian bordeland. III ISAG, Saint –Malo, France. 243-246.

Sobiesiak, M., Alvarado, L., Vásquez, R., 2002. Sismicidad reciente del oriente de Venezuela. XI Congreso Venezolano de Geofísica (in CD-Rom).

Sutherland, R., 1999. Cenozoic bending of New Zealand basement terranes and Alpine fault displacement: a brief review. New Zealand Journal of Geology and Geophysics 42, 295-301.

Wiemer, S., 2001. A software package to analyze seismicity: ZMAP. Seismological Research Letters 72, 374-383.

Zoback, M.L., Zoback, M. 1980. State of stress in the conterminous United States. J. Geophys. Res. 85, 6113-6156.

Near surface attenuation in Venezuela

Carolina Granado Ruiz and Jens Havskov

Abstract

Spectral analysis has been made using 200 earthquakes in Venezuela with magnitudes from 1.1 to 2.5 Mw to determine the near surface attenuation κ and coda Q attenuation. The study was using vertical component seismograms recorded in broad band stations. The estimated values of coda Q exhibit a clear dependence on frequency and window lengths. The most reliable coda Q results were taken to calculate kappa in a frequency band from 3 -12 Hz giving an average value of near surface attenuation κ= 0.099 ± 0.031 which has been compared with regional values in the Caribbean. The study concludes that near surface attenuation in Venezuela is high compared to other regions.

1.-Introduction

Venezuela is an area of moderate to high seismic activity. The seismicity regime corresponds to a complex tectonic framework consisting of an interaction area between the South America and Caribbean plates located in Northern Venezuela where a major right lateral strike fault system and a subduction zone are present. Western Venezuela shows a seismicity activity in connection with a very complex pattern of plate and block motions between three major plates producing a zone of continental deformation into Venezuela Andes (Figure 1).

A wide variety of sedimentary, igneous and metamorphic rocks are present along the main fault systems in Venezuela. The complex geological and seismotectonics settings are basic elements to consider regarding the attenuation of propagation of seismic waves.

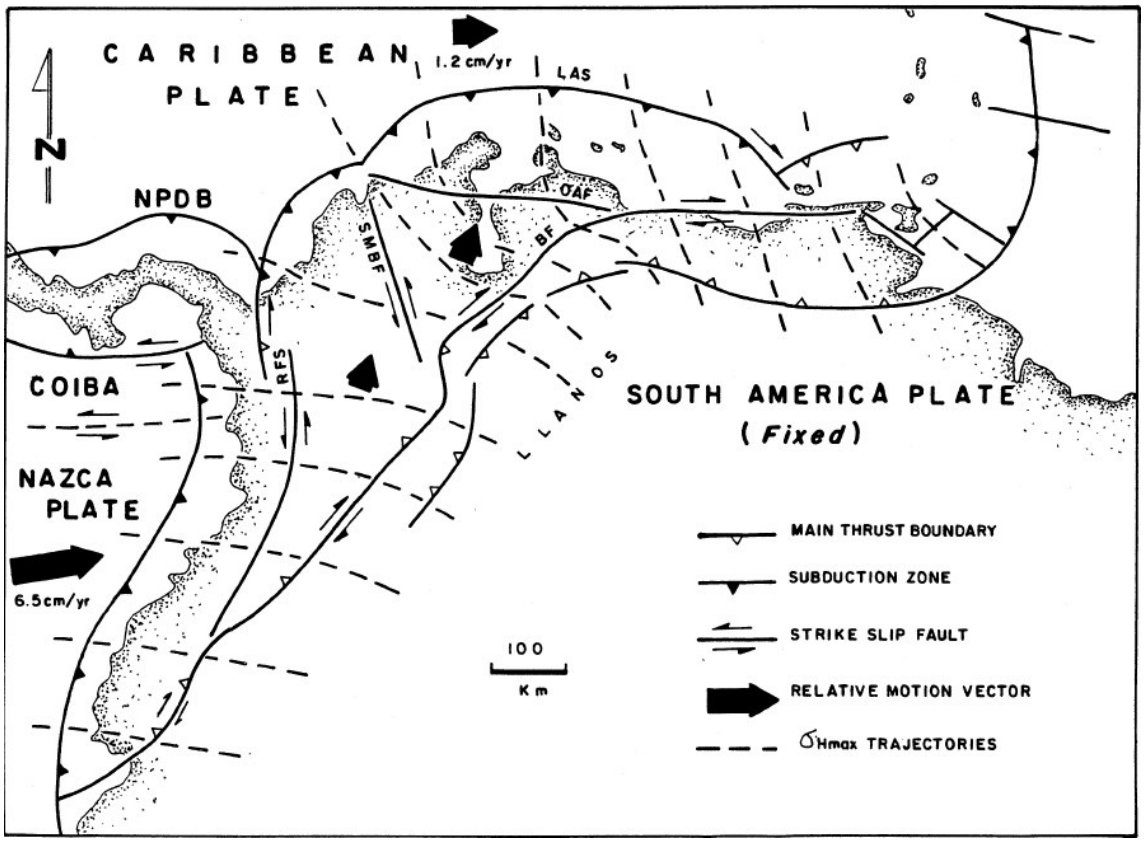

Figure 1: Regional tectonic map of north western South America showing interaction between the Caribbean, South American and Nazca plates (Audemard F.E and Audemard F.A, 2002)

In such a complex tectonic setting, it can be expected that seismic attenuation will have a regional variation. The quality factor Q is considered constant for frequencies between 0.001 and 1 Hz and increasing with frequency above 1 Hz (Lay and Wallace, 1995). This increase could be due to complex tectonic settings and crustal heterogeneity.

The earthquake scaling laws are important to define the relationship between earthquake size (seismic moment or magnitude), fault dimensions and stress drop. In order to get an estimation of basic source parameters used in scaling laws, such as corner frequency and seismic moment, processing of earthquake spectrum is often done. A particular problem for determining source parameters is related with near surface

attenuation, where Q presents significant lower values close to the surface. This can considerably affect the spectrum of small earthquakes misleading a true calculation of the corner frequency. Therefore, the determination of source parameters and the consistency of self similarity principle are affected by near surface attenuation.

Several studies have found that apparent corner frequencies of microearthquakes are significantly higher for borehole instruments than for seismometers (Hauksson et al., 1987; Frankel and Wennerberg, 1989). These observations support the idea that substantial attenuation occurs in the near surface rocks affecting the estimation of corner frequencies for surface recordings. Therefore, the near surface attenuation limits the spectral content at high frequencies. A correction for the real value of the corner frequency must be applied to get a more reliable estimation of seismic moment and stress drop.

Abercrombie (1995) investigated near-surface attenuation at the Cajon Pass Scientific drill hole and found that near-surface attenuation was high with $Q_P \sim 27 \pm 8$ at the borehole site (composed of miocene arkosic sandstone and conglomerate overlaying granite) and ~ 50 at a nearby granite site, averaged over the upper 3 km, and measured between 5 and 100 Hz; $Q_S \sim 21 \pm 7$ at both sites, compared with Q ~ 1000 below 3 km. At least 90% of the attenuation of amplitudes from earthquakes within 15 km of the borehole occurred in the upper 3 km.

In seismic hazard analysis a crucial input knowledge is the attenuation that influences the decay in amplitude from the source to the site taking into account the effects of quality factor Q and parameter κ .

Venezuela at the present moments does not count on a significant number of attenuation studies. This situation has forced the use of indirect methods for the derivation of attenuation relations such as studies of intensities from historical earthquakes or

isoseismals maps (Díaz, 2000). It is therefore important to study small events in Venezuela to improve the knowledge of attenuation, in particular near surface attenuation. Seismic events considered small are particularly affected by attenuation along the path and near surface attenuation since higher frequencies for small sources are sensitive to these factors (Abercrombie, 1995).

A study of coda wave attenuation in Northeastern Venezuela show significant differences using events at shallow and intermediate depths, the shallow events present a much stronger attenuation (Ugalde et al, 1998). Results in three different frequency bands show the variation of Q from ~332 for 2.5 to 4.5 Hz, ~766 for the range 4.5 – 8.5 and ~1960 for 8.5 to 16.5 Hz.

No investigation regarding near surface attenuation have been conducted in Venezuela. New data is now available form the recently installed broad band network of FUNVISIS (Venezuelan Foundation for Seismological Research). This data will be used in spectral analysis of small earthquakes in order to determine near surface attenuation. The aim of this paper is thus to investigate the near surface attenuation parameter κ using seismograms of small earthquakes with magnitudes varying between 1.1 to 2.5 Mw. (see later for the need for using small events). Since the method described in section 4 of the present paper requires an approximate knowledge of Q between source and receiver, a preliminary coda Q study will also be made.

2.- Near surface attenuation and self similarity

The faulting parameters of most earthquakes are connected in a systematic way. The interdependence of such parameters constitutes the base for scaling laws. There are observations about the nature of self similar behaviour among many geological processes

(Turcotte, 1989). In seismology, the notion of self-similarity is based on the assumption that the physics of material failure is identical for large and small earthquakes. This fact implies that stress drop is constant for all earthquakes since stress drop is proportional to fault average slip divided by its length (Stein and Wysession, 2003). Both moderate and large seismic events are self similar although the thicknesses of the seismogenic crust seems to be a geometrical constraint in the case of large earthquake rupture propagation resulting in a change in scaling relationships for very large magnitudes (Shimazaki, 1986).

Some studies report a dependence of stress drop on earthquake size and an apparent breakdown in self-similarity (Archuleta et al., 1982; Hasegawa, 1983; Haar et al., 1984; Shi et al., 1998). This breakdown has been interpreted as consequence due to limitations of the minimal earthquake source dimension caused by the width of the fault zone (Aki, 1987). Stress drop appears to be constant only down to a threshold moment about 10^{13} to 10^{14} Nm. Below this limit, earthquakes appear to have a constant dimension (of about 100 m) and stress drop appears to decrease with seismic moment.

Several studies of attenuation have found very low Q values a few kilometres below the ground surface (Anderson and Hough, 1984; Malin et al., 1988; Abercrombie, 1997). These results seem to confirm that the apparent breakdown in self-similarity is a consequence of significant attenuation in the subsurface. Hough et al. (1988) analyzed data from southern California to study attenuation. They found that high frequency exponential decay of acceleration spectra (from 15 to 100 Hz) was caused by a frequency independent low Q-value in the few kilometres immediately below a station.

Studies using spectrum of SH waves have observed that Q seems to be frequency dependent below about 4 km and attenuation in the upper 4 km is essentially independent

of epicentral distance since for sources below 4 km, the waves travel nearly vertical regardless of distance (Singh et al. 1982)

Another example was in studies conducted by Hanks (1982) and Hough (1996), where the apparent breakdown of self-similarity seemed to be due to attenuation in the near-surface rocks (down to approximately 4 km) that mislead the true estimation of the corner frequencies for small earthquakes.

According to Anderson and Hough (1984), Q is independent of frequency in the shallow crust and strongly dependent on depth in the near surface layers. These authors examined a number of accelerogram concluding that Q increased rapidly with depth in the shallow crustal layers. The observation about the frequency independent seems to be valid for Q_P as well as for Q_S.

Distortion of P and S wave microearthquake spectra and measurements of Q obtained from seismograms recorded in boreholes located in California revealed for instance that the quality factor of shear wave attenuation Q_S was 9, averaged over the upper 500 m of ophiolite (Malin et al. 1988) and Q_S was 9 between 0 and 150 m and approximately 26 between 150 and 300 m (Aster and Shearer, 1991).

Laboratory studies of attenuation found that both Q_P and Q_S increase rapidly with increasing pressure up to about 500 - 1000 bars (that corresponds to approximately 4 km depth). This pressure dependence of attenuation has been interpreted as resulting from the closure of cracks in the rocks with increasing pressure (Johnston et al. 1979). Mori and Frankel (1991) observed a significant decrease in scattering attenuation below about 5 km in southern California. Laboratory and field results thus combine to suggest that the level of attenuation in near surface rocks (low pressure) is dominated by the increase in fracture

content and probably other heterogeneities with decreasing overburden, and not simply the rock type (Abercrombie, 1997).

In general the quality factor Q in near surface rocks is frequency independent and has a very low value immediately below the surface but rapidly increases with depth. The attenuation of the near surface layers can be described by the near-surface attenuation parameter κ as given in the amplitude attenuation equation:

$$A(f,t) = A_0 e^{-\pi f \kappa} e^{-\frac{\pi f t}{Q(f)}} \qquad (2.1)$$

Under the assumption that Q(f) is not dominating the spectrum and that the corner frequency is high (small earthquakes), the near surface attenuation will dominate the spectral decay and the real corner frequency cannot be seen, showing instead an apparent corner frequency created by the near surface attenuation. If we define the corner frequency f_κ as the frequency where the spectral level has reached 0.5 as a result of the effect of near surface attenuation, then f_κ can be calculated as

$$e^{-\pi \kappa f_\kappa} \qquad \text{giving} \qquad f_\kappa = \frac{0.223}{\kappa} \qquad (2.2)$$

If e.g. κ=0.015, f_κ~15 Hz, and it will not be possible to obtain the true source corner frequency for small earthquakes (ML < 3.0) without correction for κ. To be able to correct for κ, it is necessary to have a good signal to noise ratio of the high frequency part of the spectrum. In order to get a reliable source corner frequency for small earthquakes, κ is a very critical parameter with a direct influence in the scaling laws description for small magnitudes.

3. - Tectonic setting

The seismotectonics of the north-western part of South America is a geologically interesting area where a deformation occurs by interactions of the South America, Nazca and Caribbean plates (Figure 1). Information compiled by GPS measurements allow us to determine that the South America plate as fixed and that the Caribbean plate motion is towards the east-southeast, while the Nazca plate motion is roughly towards the east, and the northern Andes motion is towards the northeast (Corredor, 2003). The Venezuela Andes is characterized by a complex pattern of northeast and southeast trending thrust and strike slip fault earthquakes. The major fault system in Venezuela Andes is well known as Mérida Andes with Boconó fault system as the major feature NE-SW trending dextral fault that with a length of about 500 km (Audemard and Audemard, 2002) (Figure 2). It runs slightly oblique to the Mérida Andes chain axis and bounds the Caribbean Coast range of northern Venezuela on the west. Most of the largest earthquakes occur in Mérida Andes and are located along the Boconó Fault. In North Western Venezuela, a right lateral fault system named Oca-Ancón represents a considerable seismic source where paleoseismological evidence reveals traces of significant earthquakes with magnitude Ms over 7.4 (Audemard, 2000).

The central part of Venezuela is considered a broad deformation zone characterized by a right lateral and thrust faulting mechanism with an accretionary crust where the Caribbean Mountain thrust belt reveals its compressional tectonics as a consequence of collision processes (Bosch and Rodriguez, 1992). The main active faults in this zone are La Victoria and San Sebastián faults (Figure 2).

The seismically active El Pilar fault is the predominant strike slip fault in eastern Venezuela. Cretaceous sediments and igneous rocks are accumulated in the north of this

tectonic area. This region presents an oblique collision between the South America plate and the Caribbean plate which originates a north-west dipping subduction (Baumbach et al, 2004).

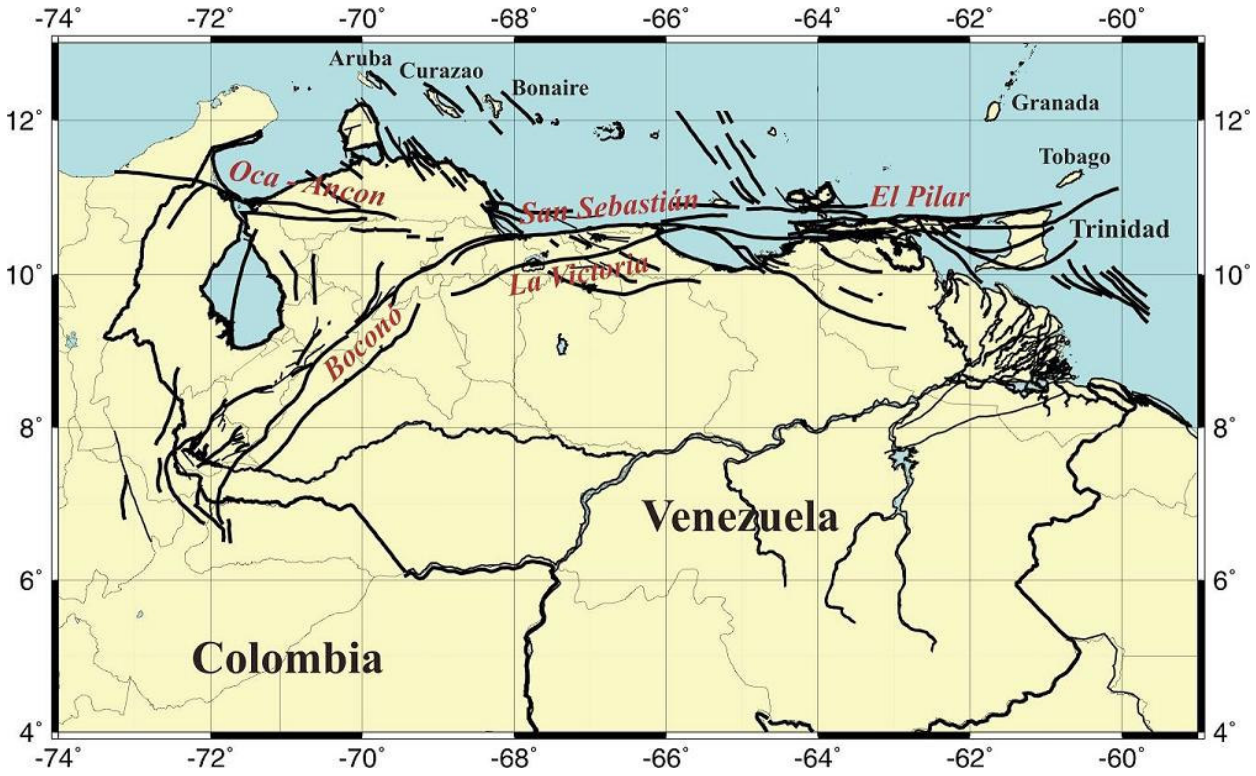

Figure 2: Venezuela main fault systems compiled by FUNVISIS based on Beltrán, 1993

4. - Method

Seismic waves attenuate when their amplitude decreases as they propagate. This attenuation is described as

$$A(f,t) = A_0 e^{-\frac{\pi f t}{Q(f)}} \tag{4.1}$$

where A_0 is the initial amplitude and Q is the quality factor. Several physical phenomena are described in terms of Q or Q^{-1}. Q can be used to describe the decay of an oscillation

and physical properties of the system that causes attenuation (Lay and Wallace., 1995). Q is most often a frequency dependant for f > 1 Hz and can be related to the loss of seismic energy in heat. Q is defined according to the type of wave. There is Q for surface waves, body waves, coda Q and crustal phases L_g (Stein and Wysession, 2003)

Since the near surface layers (1-3 km) generally have a much lower Q than the rest of the path, and therefore tends to filter out high frequency energy (f > 10-20 Hz). The attenuation can be separated in two terms:

$$A(f,t) = A_0 e^{-\pi f \left(\frac{t_1}{Q_1(f)} + \frac{t_2}{Q_2(f)}\right)} \tag{4.2}$$

t2 represents the travel time in the near surface layers and Q2 the attenuation and t1 and Q1 represent the same quantities for the rest of the path. The near surface attenuation is usually observed to be frequency independent and the effect can therefore be quantified with the constant $\kappa = t_2/Q_2$:

$$A(f,t) = A_0 e^{-\pi f \kappa} e^{-\frac{\pi f t_1}{Q_1(f)}} \tag{4.3}$$

Since $t1 >> t_2$, we will replace t_1 with t and Q_1 with Q and the general expression for the amplitude decay to use in local studies is then

$$A(f,t) = A_0 e^{-\pi f \kappa} e^{-\frac{\pi f t}{Q(f)}} \tag{4.4}$$

It will be assumed that κ is frequency independent and Q is frequency dependent on the form

$$Q(f) = Q_0 f^{\alpha} \tag{4.5}$$

Where α usually is in the range from 0.5 to 1.0. Taking the natural logarithm of (4.4), we get

$$\ln(A(f,t)) = \ln(A_0) - \pi f \kappa - \pi f \frac{t}{Q(f)} \tag{4.6}$$

We will assume that the signals are generated by earthquakes following the Brune source model (Brune, 1970) and therefore have a displacement source spectrum S of the form

$$S(f) = \frac{K}{1 + (\frac{f}{f_0})^2} \tag{4.7}$$

Where K is a constant which is proportional to the seismic moment and f_0 is called the corner frequency. The spectrum is constant for $f < f_0$ and decays as f^{-2} for $f > f_0$. The corner frequency for small earthquakes is affected by κ.

Equation (4.7) can be regarded as the representation of the spectral content of a source signal having a travel time t. If the signal is generated by an earthquake and only part of the spectrum is used, a plot ln(A(f,t)) vs. f, will show a straight line with slope of $-\pi(\kappa+t/Q)$ for $f_0 > f$, assuming Q is frequency independent. If t/Q is small, the slope will be directly proportional to κ as seen from

$$m = -\pi(\kappa + \frac{t}{Q}) \tag{4.8}$$

In order to get a reliably determination of κ, short hypocentral distances should be used in order to minimize the effect of Q. If Q(f) is known, the spectrum can first be corrected for Q(f), and κ determined directly. A good test of the result is therefore to determine κ using different distances. If Q(f) is correct, the value of κ obtained should be the same. It is thus important to use a reasonably accurate Q value. Since almost no Q-values are known for Venezuela, a preliminary coda Q study is also done. The standard coda-q method is used to determine Q(f). The basic principle behind this method is the

consideration that coda waves decrease in amplitude due to geometrical spreading and attenuation. Therefore, equation (4.4) can be written as

$$A(f,t) = t^{-\beta} A_0 e^{-\pi f \kappa} e^{-\frac{\pi f t}{Q(f)}} \quad (4.9)$$

Where the geometrical spreading parameter β is 1 for body waves and 0.5 for surface waves. Normally coda waves are assumed to be body waves. Taking the logarithm, (4.9) can be written

$$\ln(A(f,t) + \beta \ln t = (\ln(A_0) - \pi f \kappa) - \frac{tf\pi}{Q(f)} \quad (4.10)$$

Plotting the envelope of ln(A(f,t) +βln(t) as a function of t for a given frequency (by band pass filtering the signal), gives a straight line with slope –πf/Q(f) and thus Q(f) can be determined. The determination of Q is not affected by κ or soil amplification. Since near surface attenuation limits the spectral content at high frequencies, the displacement spectrum will show a lower frequency named f_κ in comparison to the real f_0. the observe corner frequency can therefore not be used as a frequency limit since it is likely to be lower than the real source corner frequency. An empirical relation (Havskov, 2003) was therefore used to check the data for corner frequency

$$\text{Log}(f_0) = 2.33 - 0.5Mw \quad (4.11)$$

This relation assumes a stress drop of 5 bars and the Brune source relation (6). Higher stress drops would give higher corner frequency. In order to get a reasonable

frequency range to work with, events should be smaller than 2.5 corresponding to a corner frequency of 15 Hz

Both the coda Q and κ was determined using the SEISAN software package 8.0 (Havskov and Ottemöller, 2003

5.- Data processing and results

The digital data used in this investigation were recorded by broad band stations. A total of 200 seismic events were selected from the data base of FUNVISIS. The criteria for such selection is based on epicentral distances less than 100 km and a magnitude less than 2.5 since the study aim is estimation of near surface attenuation. The earthquakes were recorded in 2003 between July 1st and December 15th. Magnitudes recorded for these events vary from 1.1 to 2.5 Mw with some events reported with coda magnitude. Six stations and 200 events with three components seismometers from FUNVISIS satisfied the required criteria. However, in the present study, the events recorded only on vertical components have been used since vertical component signals are less affected by local soil amplification than horizontal component signals. The station parameters of the stations that satisfy the criteria are listed in Table 1 and their locations are marked on Figure 3. Sampling rate in this network is 100 samples per second.

Table 1: Parameters of seismological stations

Station code	Station name	Latitude (°N)	Longitude (°W)	Altitude (m)
BIRV	Birongo	10.28	66.16	200
CRUV	Carúpano	10.36	63.11	608
CURV	Curarigua	10.00	69.57	750
GUNV	Guanaco	10.08	62.56	60
ITEV	Isla los Testigos	11.21	63.07	13
JACV	Jacura	11.05	68.50	369

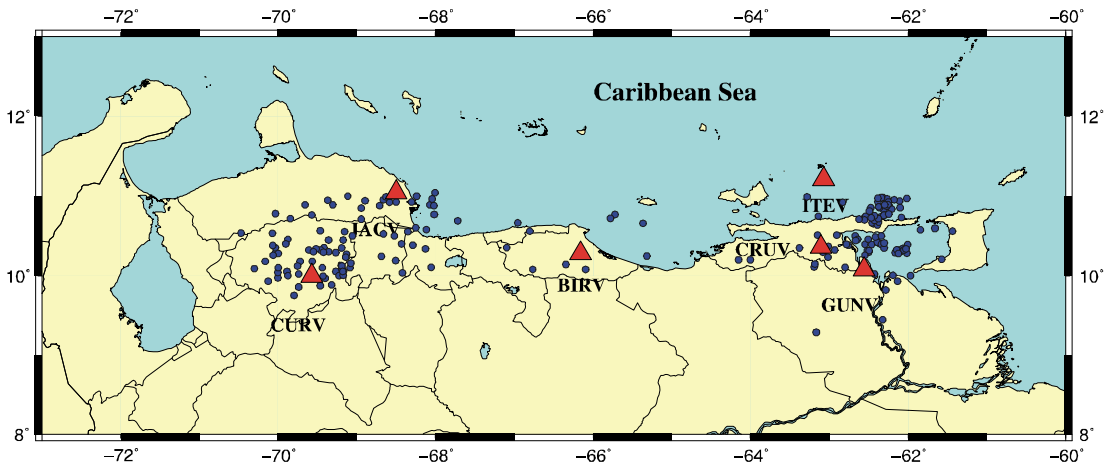

Figure 3: Broad band stations locations and epicentral distribution of selected seismic events

5.1 Estimation of coda Q

Several tests were applied using all stations in Table 1 using the program "codaq" in SEISAN software package 8.0 (Havskov and Ottemöler, 2003). However, some seismograms presented a low signal to noise ratio. A subset of the original data was selected to ensure a reliable estimation of Q. Stations BIRV, CRUV, CURV, GUNV, ITEV and JACV were chosen with a minimum signal to noise ratio equal to 3 as input value in each Q determination.

Single stations were also studied, in particular to analyze the influence of the window length on the output results, four different values were used for window length: 10, 15, 20 and 25 sec. Figure, 4 shows the results as an example for station GUNV and using the same seismic event. The following five frequency bands were used: 0.5 - 1, 1 - 2, 2 - 4, 4 - 8, 6 - 12 Hz , respectively and a minimum correlation coefficient of 0.5 to estimate average Q.

In Figure 4, the top shows the original trace and below the filtered coda windows for the frequency bands previously described. The particular selected event has a magnitude 2.4 with a P wave travel time of 11.2 sec and a depth equal to 10 km. On each filtered plot, F means the centre frequency, Q is the coda Q value and Q=0 means no Q value could be calculated. CO is the correlation coefficient and finally S/N means signal to noise ratio.

Results of coda Q for these stations show the dependence of Q from frequency. Effectively, Q increases with frequency. Table 2 shows the most reliable results in four single stations to ensure a minimum quality of the data.

Table 2: Coda Q results for several frequency bands in a window length of 20 sec.
Processing parameters: Minimum correlation coefficient of each coda decay curve: 0.5
Minimum signal to noise ratio of any point in signal: 3.0. Q is assumed to be: $Q = Q_0 f^{\alpha}$

Station	0.5 - 1 Hz	1-2 Hz	2 - 4 Hz	4 - 8	6 -12 Hz	Q_0	α
CRUV	No result	97	188	224	320	62	0.72
GUNV	84	127	236	418	495	79	0.77
CURV	39	80	226	540	733	41	1.21
JACV	50	129	134	154	241	79	0.43

Average lapse time of the start time of coda window relative to origin time varies from a minimum 31.73 sec to a maximum 32.50 sec, which is a reasonable value since the initial criteria regarding the epicentral distance for selecting the earthquakes, is less than 100 km..

Figure 5 shows how Q increases with the window length. This tendency remains in five different frequency bands. While the window length seems to have an effect on Q values, the power factor α in the relation $Q = Q_0.f^{\alpha}$ does not change drastically as is shown in Table 3. The increase in Q with window length is often thought to be related to the coda waves sampling deeper layers of the crust (Kvamme and Havskov, 1989)

For simplicity, to get more reliable Q-values, average Q values for all stations were calculated (Table 3). Results in Table 3 are reasonable by comparison with previous studies in Venezuela. For instance, in Eastern Venezuela a result for Q at 10 Hz is ~ 330 (Ugalde et al, 1998). Table 2 shows values of Q equal to 342 and 391 for window lengths 15 sec and 20 sec respectively.

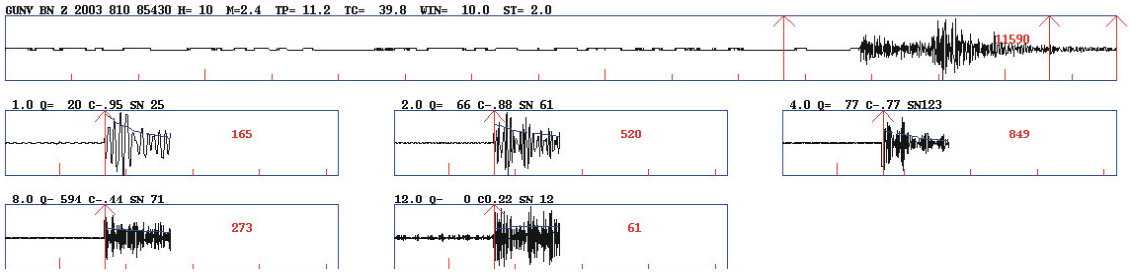

. (A)

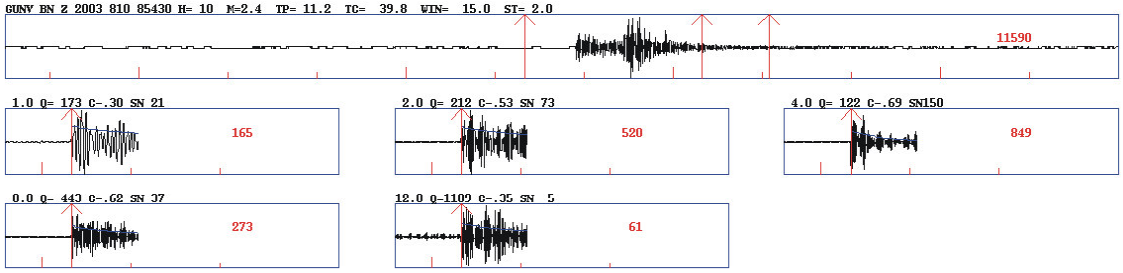

(B)

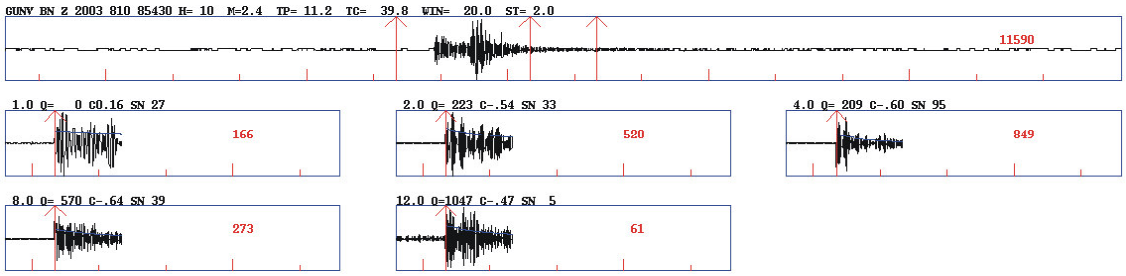

(C).

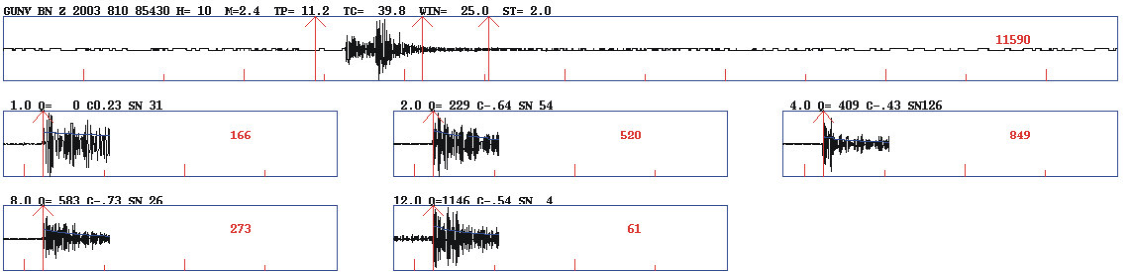

(D)

Figure 4: Examples of Q results for station GUNV in different window lengths. (A) Window length: 10 sec (B) Window length: 15 sec. (C) Window length: 20 sec (D) Window length: 25 sec.

Table 3: Average value of Q for every window length. N is the total number of observations made for each central frequency

	Window lengths (sec)							
	10		15		20		25	
$Q= Qo\ f^{\alpha}$:	$Q=28\ f^{1.03}$		$Q=43\ f^{0.97}$		$Q=65\ f^{0.84}$		$Q=78\ f^{0.81}$	
Frequency band (Hz)	Q	N	Q	N	Q	N	Q	N
0.5 - 1	20	16	31	8	49	7	59	5
1 - 2	39	20	60	24	87	27	103	30
2 - 4	82	31	118	33	156	29	181	26
4 - 8	101	18	143	24	184	16	213	16
6 - 12	253	15	342	13	392	13	441	8

In terms of κ calculations, the Q values used as an input were chosen according to window lengths 15 sec and 20 sec because these are the most reliable results. This window length is also a common value used in many coda Q studies (Havskov et al., 1989; Kvamme and Havskov, 1989, Grandison and Havskov, 2004).

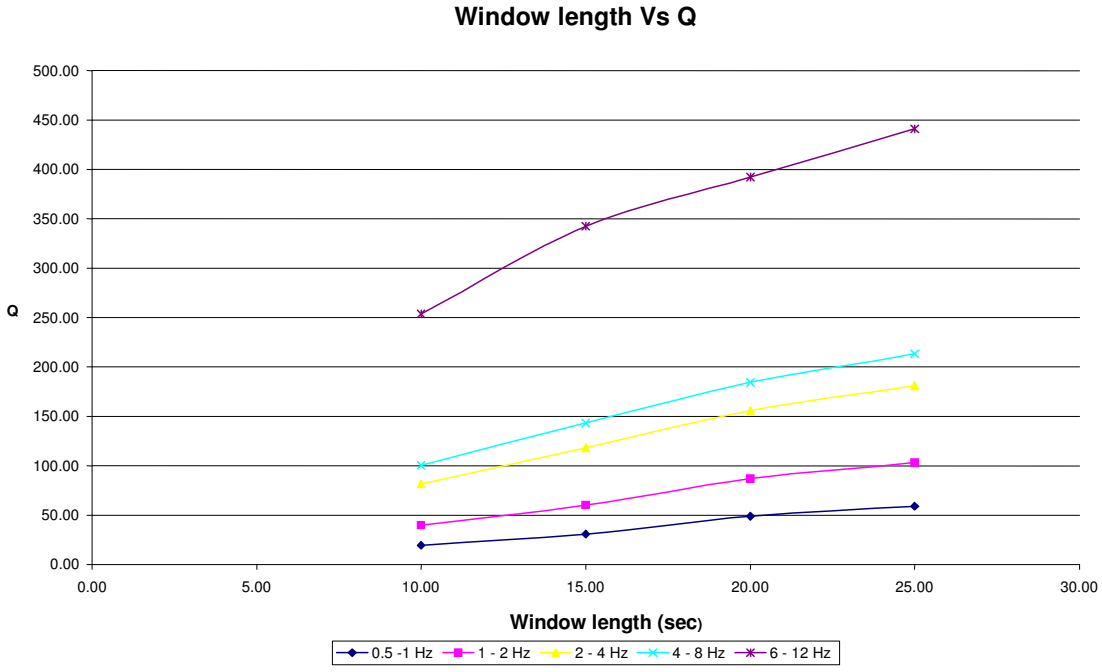

Fig 5: Window length Vs Q for several frequency bands

5.2 Estimation of κ

The program spec in SEISAN was used for making spectra of several seismic signals. Estimation of parameter κ at seven broad band stations with two different window lengths using the most reliable relations for coda Q are presented in Table 3:

Table 4: κappa results for Q= 43 $f^{0.97}$ and Q=65$f^{0.84}$. The terms "sd" indicate standard deviation and "n" number of displacement spectra at every station. Frequency band : 3- 12 Hz

	Q_0= 43 α=0.79 Window lenght= 15						α=0.48 Window lenght= 20					
	P arrival time			S arrival time			P arrival time			S arrival time		
Stations	κ (s)	sd	n	κ (s)	sd	n	κ (s)	sd	n	κ (s)	sd	n
BIRV	No results			No results			No results			No results		
CRUV	0.099	0.027	22	0.113	0.029	16	0.095	0,026	22	0.105	0.031	13
CURV	0.071	0.037	8	0.078	0.032	16	0.076	0,043	6	0.073	0.037	13
GUNV	0.098	0.026	39	0.127	0.026	39	0.096	0,029	49	0.118	0.028	32
ITEV	No results			0.089	0.040	14	0.074	0,039	7	0.080	0.034	3
JACV	0.114	0.020	6	0.165	0.025	5	0.117	0,018	8	0.156	0.023	5

For Q= 43 $f^{0.97}$, the κ parameter ranges for four of the stations roughly from 0.099 to 0.114 s for P waves and from 0.062 to 0.165 s for S waves in six stations. Thus, κ average for P waves is 0.096 s while for S waves is 0.106 s

For Q=65$f^{0.84}$ the κ parameter ranges for five of the stations roughly from 0.074 to 0.117 s for P waves and from 0.073 to 0.118 s for S waves in five stations. Thus, κ average for P waves is 0.092 s while for S waves is 0.106 s

6.- Discussion and conclusion

Results for κ have been obtained for a frequency band between 3 to 12 Hz. No significant variations in average κ for different coda Q relations have been observed. Regarding the standard deviation differences, a sample that can be comparable in terms

of P and S waves, for κ values are those under the relation $Q=65f^{0.84}$ since κ is estimated with the same number of stations. In both cases an average standard deviation of 0.031 was calculated. An average κ for P and S is 0.099 ± 0.031.

The values of κ using P waves for stations located in eastern Venezuela, GUNV and CRUV, are 0.098 ± 0.026 and 0.099 ± 0.026. These two stations are located relatively close to each other with respect to the rest of the stations (Figure 3). Both are also located in geological zones characterized by Quaternary and Cretaceous sedimentary rocks.

There are regional variations of κ in stations in western Venezuela. Stations CURV and JACV separated by a distance less than 200 km (Figure 3), show a significant difference of the κ-values with CURV station having a lower κ-value then the JACV station. Station CURV presents values more similar for P and S waves compared to JACV station, for which κ for P waves is consistently lower than for S waves (using both coda Q relations). This could indicate a more fractured rock under JACV than under CURV. This points to the possible difference in local site geological conditions for these two stations. By inspection of Figure 2, this could have some relation with the fact that these stations are located in different fault systems; i.e. the station JACV is closer to Oca-Ancón system while CURV is placed along the Boconó fault system which could indicate changes in the general surface conditions. No indication of near surface attenuation in Central Venezuela was obtained since station BIRV which is relatively closer to main fault systems in the area, San Sebastián and La Victoria, gave no results for input data under the same processing requirements than the rest of the stations.

Regarding the implications of near surface attenuation in spectral analysis, the lowest corner frequency that can be expected to be recovered, without correction for κ, can be estimated using the relation proposed in equation (2.2) and an average kappa value:

$\kappa = 0.099 \pm 0.031$ sec.

Thus, $f_\kappa = \frac{0.223}{0.099s} = 2.3$ Hz

Since a direct effect of the near surface attenuation is to limit the spectral content at high frequencies, this will give a dramatic effect on the estimation of corner frequency for smaller events unless it is possible to correct κ. This is often not the case since there is simply not enough high frequency in the earthquake signal which will be below the noise level.

A comparison of the kappa values with other regions in America indicate that the near surface attenuation in Venezuela seems to be stronger (Table 5)

Table 5: Comparison of Venezuela κ with other regions in America.
1) Boore and Joyner, 1997 and Raoof et al, 1999. 2)Atkinson and Boore, 1998. 3) Moreno, 2002. 4)Grandison and Havskov, 2004.

Region	κ
1) California, western USA	0.035
2) Eastern North America	0.006
3) Cuba	0.043
4) Jamaica	0.060
Venezuela	0.099

Considering the standard deviation in the average estimation of κ, the near surface attenuation can be compared with the results for Cuba and Jamaica. These countries are

part of the Caribbean plate which is considered a large volcanic plateau subjected to a transcurrent kinematics (Leroy and Mauffret, 1996).

Since the sample of stations that satisfy the imposed criteria to ensure high quality is relatively small, this study can be improved. With more data available, distributed in a more uniform manner along the main active fault systems in Venezuela as well as to the south where an older lithosphere is formed and high competent rock can be found, it should be possible to get a better correlation of tectonics to attenuation.

As a summary conclusion we have found that the Venezuelan near surface attenuation is high with average value $\kappa = 0.099 \pm 0.031$ with $Q=65f^{0.84}$ implying a dramatic effect for the estimation of the corner frequency in spectral analysis of smaller earthquakes.

References

Abercrombie, R. E., 1995. Earthquake source scaling relationships from -1 to 5 M_L using seismograms recorded at 2.5-km depth. J. Gephys. Res. 100, 24015-24036.

Abercrombie, R. E., 1997. Near-surface attenuation and site effects from comparison of surface and deep borehole recordings. Bull. Seism. Soc. Am. 87, 731-744.

Aki, K., 1987. Magnitude-Frequency Relation for Small Earthquakes: A Clue to the Origin of f_{max} of Large Earthquakes. J. Gephys. Res. 92, 1349-1355.

Anderson, J. G., Hough, S., 1984. A model for the shape of the Fourier amplitude spectrum of acceleration at high frequencies. Bull. Seism. Soc. Am. 74, 1969-1994.

Archuleta, R. J., E. Cranswick, C. Mueller, and P. Spudich, 1982. Source Parameters of the 1980 Mammoth Lakes, California, Earthquake Sequence. J. Gephys. Res. 87, 4595-4607.

Aster, R. C., Shearer, P.M., 1991. High-frequency borehole seismograms recorded in the San Jacinto fault zone, southern California: Part 2. Attenuation and site effects. Bull. Seism. Soc. Am. 81, 1081-1100.

Atkinson, G., Boore, D., 1998. Evaluation of models for earthquake source spectra in eastern North America. Bull. Seism. Soc. Am. 88, 917-934.

Audemard, F.A., 2000. Major active faults of Venezuela. Proceedings 31st International Geological Congress, Rio de Janeiro, Brasil, 4 pp. (extended abstract in CD-Rom).

Audemard, F.E., Audemard, F.A., 2002. Structure of the Mérida Andes, Venezuela relations with the South America-Caribbean geodynamic interaction. Tectonophysics 345,299-327.

Baumbach, M., Grosser, H., Romero, G., Gonzales, J., Sobiesiak, M., Welle, Wolfgang, W., 2004. Afterschock pattern of the July 9, 1997 Mw=6.9 Cariaco earthquake in Northeastern Venezuela. Tectonophysics 379, 1-23.

Boore, D., Joyner, W., 1997. Site amplifications for generic rock sites. Bull. Seism. Soc. Am. 87, 327-341.

Bosch, M., Rodríguez, I., 1993. North Venezuelan collisional crustal block: The boundary between the Caribbean and South American plates. Journal of South American Earth Sciences 6,133-143.

Corredor, F., 2003. Seismic strain rates and distributed continental deformation in the northern Andes and the three-dimensional seismotectonics of northwestern South America. Tectonophysics 372, 147-166.

Díaz, J.F., 2000. Estudio de un plan rector para el desarrollo de edificaciones sismo-resistentes en el área norte del edo. Anzoátegui. X Congreso Venezolano de Geofísica (in CD-Rom).

Frankel, A., Wennerberg, L., 1989. Microearthquake spectra from the Anza, California seismic netvork: Site responce and source scaling. Bull. Seism. Soc. Am. 79, 581-609.

Grandison, M., Havskov, J., 2004. Crustal attenuation for Jamaica, West Indies. Journal of Seismology, 00, 1-17.

Haar, L. C., Fletcher, J.B., Mueller, C.S., 1984. The 1982 Enola, Arkansas, swarm and scaling of ground motion in the eastern United States. Bull. Seism. Soc. Am. 74, 2463-2482.

Hanks, T. C., 1982. f_{max}. Bull. Seism. Soc. Am. 72, 1867-1879.

Hasegawa, H.S., 1983. Lg spectra of local earthquakes recorded by the Eastern Canada Telemetric Network and spectral scaling. Bull. Seism. Soc. Am. 73, 1041-1061.

Hauksson, E., Teng, T., Henyey, T., 1987. Results from a 1500 m deep, three-level downhole seismometer array: site response, low Q values and f_{max} . Bull. Seism. Soc. Am. 77, 1883-1904.

Havskov, J., Malone, S., McClurg, D., Crosson, R., 1989. Coda Q for the state of Washington. Bull. Seism. Soc. Am. 79, 1024-1038.

Havskov, J., 2003. Q and spectral analysis in SEISAN. In SEISAN distribution, University of Bergen.

Havskov, J., Ottemöller, 2003. SEISAN software package 8.0. Seismic Analysis Software. Earth Science Department, University of Bergen.

Hough, S. E., Anderson, J. G., Brune, J., Vernon, F., Berger, J., Fletcher, J., Haar, L., Hanks, T., Baker, L., 1988. Attenuation near Anza, California. Bull. Seism. Soc. Am. 78, 672-691.

Hough, S. E., 1996. Observational constraints on earthquake source scaling: understanding the limits in resolution. Tectonophysiscs 261, 83-95.

Johnston, D., Toksoz, M., Timur, A., 1979. Attenuation of seismic waves in dry and saturated rocks: II. Mechanisms. Geophysics 44, 691-711.

Kvamme, L., Havskov, J., 1989. Q in southern Norway. Bull. Seism. Soc. Am., 79, 1575-1588.

Lay, T. And Wallace, T. 1995. Modern global seismology. San Diego. Academic Press

Leroy, S., Maufret, A., 1996. Intraplate Deformation in the Caribbean region. J.Geodynamics 21, 113-122.

Malin, P., Waller, J., Borcherdt, R., Cranswick, E., Jensen, E., Van Schaack, J., 1988.Vertical seismic profiling of Oroville microearthquakes: velocity spectra and particle motion as a function of depth. Bull. Seism. Soc. Am. 78, 401-421.

Moreno, B., 2002. Crustal structure and seismicity of Cuba and web-based applications for earthquake analysis. PhD Thesis, University of Bergen.

Mori, J. Frankel, A., 1991. Depth dependent scattering shown by coherence estimates and regional coda amplitudes, EOS (Supplement) 72, 344.

Roof, M., Hermann, R., Malagnini, L., 1999, Attenuation and excitation of three-component ground motion in Southern California. Bull. Seism. Soc. Am. 89, 888-902.

Shi, J., Kim, W., Richards, P., 1998. The corner frequencies and stress drop of intraplate earthquakes in the Northeastern United States. Bull. Seism. Soc. Am. 88, 531-542.

Singh, S., Aspel, R., Fried J., Brune, J., 1982. Spectral attenuation of SH waves along the Imperial fault. Bull. Seism. Soc. Am. 72, 2003-2016

Stein, S., Wysession, M., 2003. An introduction to seismology, earthquakes, and earth structure. Malden. Blackwell Publishing.

Turcotte, D., 1989. Fractals in geology and geophysics. Pure. Appl. Geophys 131, 171-196.

Ugalde, A., Pujades, L., Canas, J.A., Villaseñor, A., 1998. Estimation of the intrinsic absorption and scattering in Northeastern Venezuela (southeastern Caribbean) using coda waves. Pure and applied Geoph. 153, 685-702.